Contribution of CD8$^+$ T Cells to Control of *Mycobacterium tuberculosis* Infection[1]

Dhruv Sud,*‡ Carolyn Bigbee,† JoAnne L. Flynn,† and Denise E. Kirschner[2]*‡

Tuberculosis is the number one cause of death due to infectious disease in the world today. Understanding the dynamics of the immune response is crucial to elaborating differences between individuals who contain infection vs those who suffer active disease. Key cells in an adaptive immune response to intracellular pathogens include CD8$^+$ T cells. Once stimulated, these cells provide a number of different effector functions, each aimed at clearing or containing the pathogen. To explore the role of CD8$^+$ T cells in an integrative way, we synthesize both published and unpublished data to build and test a mathematical model of the immune response to *Mycobacterium tuberculosis* in the lung. The model is then used to perform a series of simulations mimicking experimental situations. Selective deletion of CD8$^+$ T cell subsets suggests a differential contribution for CD8$^+$ T cell effectors that are cytotoxic as compared with those that produce IFN-γ. We also determined the minimum levels of effector memory cells of each T cell subset (CD4$^+$ and CD8$^+$) in providing effective protection following vaccination. ***The Journal of Immunology,*** **2006, 176: 4296–4314.**

Tuberculosis (TB)[3] is one of the most pervasive diseases today, with over one-third of the world population infected with *Mycobacterium tuberculosis* (Mtb) and 2 million deaths every year. The unique nature of Mtb pathogenesis results in only 5–10% of infected persons developing active tuberculosis within 1–5 years postinfection (1), whereas the remainder experience latent infection, which is generally accepted as a state of equilibrium between bacteria and host. Depending on the nature and extent of the host response to infection, there may be tissue damage, fluid accumulation in the lungs, and even death (2). Thus, it is of great interest to identify mechanisms that not only determine differences in infection outcome but also those that are most influential in controlling host damage.

A cell-mediated immune response is essential for control of Mtb infection. Mtb infection initiates in the lungs, where resident macrophages take up bacteria. Mtb can effectively evade killing processes in resting macrophages, thus avoiding elimination (3). Clearance of bacteria by macrophages is in part dependent on macrophage activation by the cytokine IFN-γ secreted by CD4$^+$ T cells, CD8$^+$ T cells, and NK cells (4, 5). Infected macrophages secrete other proinflammatory cytokines such as TNF and IL-12 as well as chemokines that recruit immune cells to the site of infection (2).

Several hypotheses have been proposed to explain different outcomes of infection (i.e., active tuberculosis vs latent infection), in part based on studies of isolated components of the host response to Mtb infection in animal models. In particular, many studies focus on genetic knockout (KO) studies and/or depletion experiments (6–12). Although such methods contribute significantly to our understanding of TB, it can be difficult to analyze the breadth of the entire immune response in such models, particularly when the KO mouse succumbs quickly to TB. In addition, there are limitations to animal models, including differences between certain molecules in humans and mice, difficulty in modeling latent infection, and the possibility of KO mutations affecting other pathways.

To offer another approach, our group previously developed mathematical models that track major elements of the cell-mediated immune response to Mtb infection (13–15). The first model accounts for the dynamics of six cell populations, including macrophages (resting, infected, and activated subpopulations) and CD4$^+$ T cells (Th0, Th1 and Th2 effector subpopulations), four cytokines (IFN-γ, IL-12, IL-10, and IL-4), and two bacterial subpopulations (intracellular and extracellular mycobacteria) (15). Key regulatory mechanisms involving pathology and protection were identified, and the importance of a fine-tuned balance in immunity-regulating control of infection and tissue damage was discussed. The second model additionally considered the role of dendritic cells and the relevance of their trafficking between lung and lymph node in priming the immune response (13).

CD8$^+$ T cells and TNF are believed to participate in the immune response to Mtb infection in humans (6, 7, 16–21). The role of CD8$^+$ T cells in immunity against Mtb infection has been controversial. However, there are data supporting a role for these cells in protection against TB (9, 22–24). It has been demonstrated repeatedly that mycobacteria-specific CD8$^+$ T cells are induced in response to Mtb infection and that these cells can recognize Mtb-infected macrophages (22, 25). Cytotoxic activity of CD8$^+$ T cells includes at least two separate mechanisms: apoptosis via the Fas-FasL pathway and killing via perforin and granulysin (26). In humans, CD8$^+$ T cells can kill intracellular mycobacteria via the release of the antimicrobial peptide granulysin (27); however, this molecule is not present in the mouse. The fact that no mouse analog of granulysin exists may in part explain why CD8$^+$ T cells are

*Department of Biomedical Engineering, College of Engineering, University of Michigan, Ann Arbor, MI 48109; †Department of Molecular Genetics and Biochemistry, University of Pittsburgh School of Medicine, Pittsburgh, PA 15261; and ‡Department of Microbiology and Immunology, University of Michigan Medical School, Ann Arbor, MI 48109

Received for publication September 12, 2005. Accepted for publication December 2, 2005.

The costs of publication of this article were defrayed in part by the payment of page charges. This article must therefore be hereby marked *advertisement* in accordance with 18 U.S.C. Section 1734 solely to indicate this fact.

[1] This work was supported by National Institutes of Health Grants ROI HL62119 and ROI HL68526 (to D.E.K.) and AI37859 (to J.L.F.) and by a grant from the Ellison Medical Foundation (to J.L.F.).

[2] Address correspondence and reprint requests to Dr. Denise E. Kirschner, Department of Microbiology and Immunology, 6730 Medical Sciences Building II, University of Michigan, Ann Arbor, MI 48109-0620. E-mail address: kirschne@umich.edu

[3] Abbreviations used in this paper: TB, tuberculosis; KO, knockout; Mtb, *Mycobacterium tuberculosis*.

0022-1767/06/$02.00

not as important in the control of infection in mouse models of TB (12). The cytotoxic potential of $CD8^+$ T cells to kill infected cells (CTL activity) in vivo has been shown to be dependent on $CD4^+$ T cells in the mouse model, suggesting that the susceptibility of $CD4^+$ T cell KO mice to Mtb infection might be due in part to impaired CTL activity (10).

Mtb-specific $CD8^+$ T cells are also involved in cytokine production, particularly that of IFN-γ and TNF (28, 29). Mechanisms that regulate relative cytokine or cytolytic activity of $CD8^+$ T cells during Mtb infection are not yet known. Recent data from our laboratory indicate that there are different effector functions of $CD8^+$ T cells depending on the stage of Mtb infection (30). In addition, data from viral systems as well as our own data support the idea that cells that produce perforin do not usually produce IFN-γ (30, 31). Finally, Ag load can influence the cytotoxic vs cytokine-producing phenotypes (31, 32).

In a previous study (15) we had included the effects of TNF and $CD8^+$ T cells in an indirect (nonmechanistic) fashion. The objective of this work is to explicitly examine the effects of these two additional elements. We include both $CD8^+$ T cells and TNF, but primarily focus our analysis on the role of $CD8^+$ T cell dynamics. Other work analyzes the role of TNF in more detail (S. Marino, D. Sud, J. Chan, J. L. Flynn, and D. E. Kirschner, manuscript in preparation). We derive four additional equations describing the rate of change for each of these cell populations (including a precursor, T80 cells) and TNF. We add or modify terms in the existing model (15) to account for $CD8^+$ T cell interactions.

We apply our updated model to simulate different infection outcomes (clearance, latent infection, and active tuberculosis) and validate cell numbers, bacterial numbers, and cytokine levels with experimental data. To further corroborate the model and test the role of $CD8^+$ T cells, we perform virtual deletion studies mimicking gene KOs or depletion studies mimicking neutralization studies where a component can be eliminated for part of the infection or at specific time points. In addition, we examine the importance of each $CD8^+$ T cell subset in control of infection, which is difficult to approach in an animal model. These results add to our understanding of TB and are not obtainable via standard experimental protocols. Based on these studies, we explore the role of both $CD4^+$ and $CD8^+$ T cells in a number of vaccination schemes.

In each of these situations, a mathematical modeling approach is advantageous to simulate a multitude of possible scenarios and to generate hypotheses that can then be tested in an experimental or clinical setting.

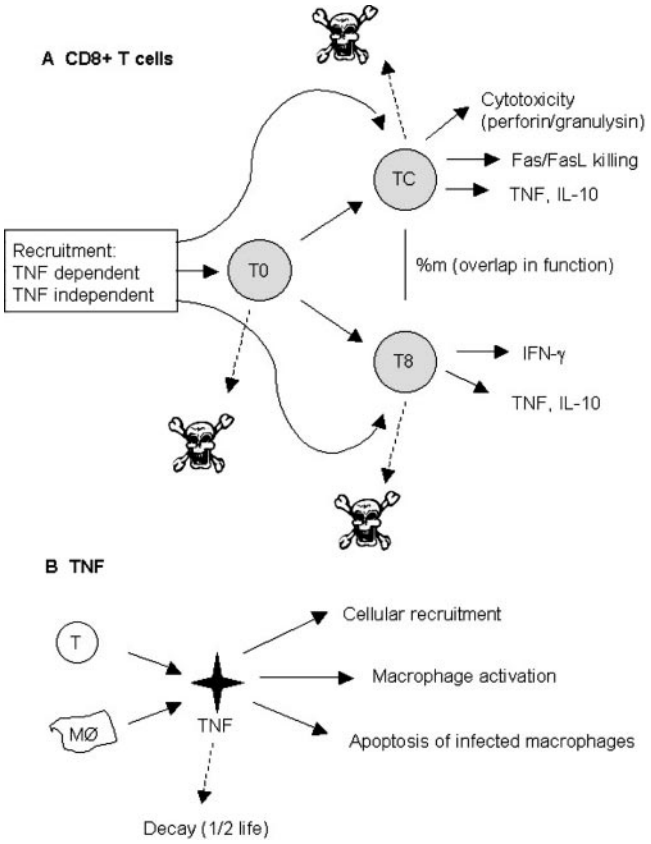

FIGURE 1. $CD8^+$ T cell and TNF dynamics. *A*, Schematic showing $CD8^+$ T cell dynamics and activities. $CD8^+$ T cells are recruited by both TNF-dependent and independent pathways. They are killed by the apoptotic action of IFN-γ and also undergo natural death (based on their half-life; both apoptosis and natural death are indicated by the skull and cross-bones symbols in the cartoon). T80 cells can differentiate into TC or T8. We allow this to occur at the site of infection because we model only the lungs and not the corresponding lymph nodes. T8 and TC can both be recruited as well. Depending on the activity of $CD8^+$ T cells, they may be classified as having effector CTL and apoptosis-inducing functions (TC cells) or a cytokine-secreting (TNF, IFN-γ, or IL-10 production) function (T8 cells). *B*, Schematic showing TNF dynamics and activities. TNF is produced by macrophages (infected and activated) as well as T cells (TH1, T8, and TC). TNF has a known half-life. Functions for TNF include macrophage and T cell recruitment, macrophage activation (along with IFN-γ and bacterial signal), and induction of apoptosis in infected macrophages.

Materials and Methods

Role of $CD8^+$ T cells

The dynamics of recruitment, turnover, and effector and cytokine-producing functions of $CD8^+$ T cells are illustrated in Fig. 1*A*. We define T8 as the class of effector $CD8^+$ T cells that produce IFN-γ but do not exhibit cytotoxic activity, and TC is defined as those cells that have CTL activity but do not produce IFN-γ. $CD8^+$ T cells are recruited in the majority as T80 cells (although a small percentage are recruited directly as T8 or TC cells). T80 cells undergo differentiation into T8s and TC cells. Although studies directly assessing cytotoxic capacity and IFN-γ production in the same cells are relatively rare, studies have indicated that perforin expression or cytotoxic function can coexist with IFN-γ expression (30–32). We allow for possible overlap of function via a parameter, m, which defines this percentage. The main roles of each of the subclasses are shown in Fig. 1*A*. The full equations with a complete explanation of the terms and how they are incorporated into the model are shown in the *Appendix*.

The action of TNF

For the purpose of focusing specifically on the $CD8^+$ T cell response in this work, we only describe how we included TNF action in our updated model and present the results of TNF dynamics elsewhere (S. Marino, D. Sud, J. Chan, J. L. Flynn, and D. E. Kirschner, manuscript in preparation). Our previously published model of Mtb infection (15) simulated cell recruitment as a function of activated and infected macrophages, the main chemokine and TNF producers. We now include an equation representing the dynamics of TNF in the system (see Fig. 1*B* and *Appendix*). We include a TNF-dependent recruitment term for both macrophages and T cells (33). We maintain the previous terms that account for additional recruitment due to chemokines not dependent on TNF (33) (Equations 1 and 4–9 in *Appendix*). We also include the effect of TNF on macrophage activation, which was previously accounted for indirectly (Equations 1 and 3 in *Appendix*). Lastly, we add an extra term into both the infected macrophage and the bacterial equations to account for the appropriate gain/loss estimates (Equations 2, 15, and 16 in *Appendix*).

Effects of IL-10 on TNF production

To examine the effect of IL-10 on TNF production, in vitro experiments with wild-type and IL-10-deficient macrophages were performed. Bone marrow macrophages (2.5×10^6 per well) were infected with Mtb strain Erdman (multiplicity of infection of 2), and TNF expression was determined at 2, 4, 8, and 24 h postinfection. Expression was measured by real-time RT-PCR for mRNA levels and by WEHI assay for TNF activity (Fig. 2). There was no difference in TNF mRNA expression or in protein production (ELISA data not shown) or activity between wild-type and

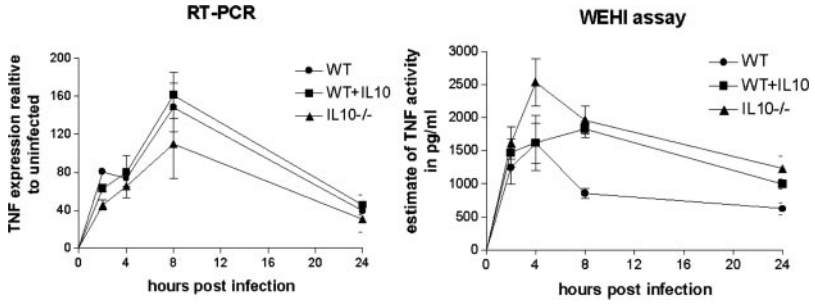

FIGURE 2. TNF production by macrophages is not strongly influenced by IL-10 in the setting of Mtb infection. Bone marrow-derived macrophages (from C57BL/6 wild-type (WT) or IL-10$^{-/-}$ mice) were infected with Mtb in vitro (multiplicity of infection of 2). IL-10 was added exogenously to wild-type macrophages in one set of samples. Supernatants were harvested, and cells were used to prepare RNA at the time points indicated. mRNA expression of TNF was determined by quantitative real-time RT-PCR and expressed as the fold increase over uninfected macrophages. The supernatants were used in a bioactivity assay with WEHI cells, and the concentration of bioactive TNF was estimated based on a standard curve with recombinant TNF. There were no significant differences between wild-type and IL-10$^{-/-}$ macrophages with respect to TNF production, and exogenous IL-10 had no significant effect on TNF production by wild-type macrophages. Error bars represent SD. The experiment was repeated twice.

IL-10$^{-/-}$ macrophages. Addition of exogenous IL-10 (10 ng/ml) to the wild-type macrophages at the time of infection also had no effect on TNF expression or production. Thus, we have not included an effect of IL-10 on TNF production in our mathematical model.

RNA isolation for TNF/IL-10 studies

RNA was isolated from the cells using the TRIzol isolation protocol with modifications. The cells were lysed in TRIzol reagent (1 ml of TRIzol per 2×10^6 cells), and then two chloroform extractions were performed. After an isopropanol precipitation, the RNA was washed with 70% ethanol and treated with RNase inhibitor (Applied Biosystems) for 45 min. After treatment at 65°C for 15 min (to fully resuspend the RNA), the RNA was cleaned, and DNA was removed with DNase using the Qiagen RNA isolation kit as directed by the manufacturer.

Real-time RT-PCR for TNF expression

RNA was reverse transcribed using the SuperScript II enzyme as directed by the manufacturer (Invitrogen Life Technologies). For real-time RT-PCR we used the relative gene expression method (34). Hypoxanthine phosphoribosyltransferase served as the normalizer, and macrophages served as the calibrator. Each primer and probe set was tested for efficiency (results were >97% efficiency for all primer/probe sets) as previously described (33). All samples were run in triplicate and with no reverse transcriptase controls on an ABI PRISM Sequence Detector 7700. Relative gene expression was calculated as 2(−cycle threshold (Ct)), where Ct = Ct (gene of interest) − Ct (normalizer) and Ct = Ct (sample) − Ct (calibrator). Results are expressed as relative gene expression to uninfected samples. The primer and probe concentrations were used as suggested by Applied Biosystems, with the final concentration of each primer at 400 nM and that of probe at 250 nM.

WEHI assay for TNF activity

In this assay, TNF induces death of WEHI cells in a dose-dependent manner (35, 36). Using this assay, the active TNF in a culture can be estimated. At indicated time points following Mtb infection, supernatants were removed and the filter was sterilized and frozen at −80°C. For the TNF activity assay, WEHI 164 subclone 13 (American Type Culture Collection) cells were placed in 96-well plates (1×10^5 cells/well in 200 μl) and grown overnight at 37°C. Medium was removed, and 100 μl of fresh medium was added to each well. Then 100-μl samples, TNF standards, and controls were added. Samples were run in triplicate and incubated overnight at 37°C. The 100-μl medium was removed from the wells, and 50 μg of MTT was added. Following a 4-h incubation at 37°C, medium was removed from the wells, and 100 μl of 0.04 N HCl/isopropanol was added. OD_{570} was read after 20 min, and TNF activity in samples was estimated by comparison with the standard curve generated using recombinant murine TNF. These controls were run concurrently for each assay.

The CD8$^+$ T cell model

Based on our description above, we derived four nonlinear ordinary differential equations to describe the dynamics of three CD8$^+$ T cell subpopulations (T80, T8, and TC) and TNF (see *Appendix*). Using similar mass action and kinetic law techniques as described (15), the interactions of these variables with other cells and cytokines were incorporated into the previous model equations (see *Appendix* and Ref. 15). Parameter values for interactions are estimated as described in the *Parameter Estimation* section of the *Appendix* and in Table III.

IFN-γ dependent apoptosis of T cells

Recent studies suggest a host homeostatic mechanism whereby activated macrophages in the presence of IFN-γ induce apoptosis of T cells to prevent excessive IFN-γ production and further activation (37–39). The need for IFN-γ as well as activated macrophages for inducing T cell apoptosis seems redundant, but experimental data indicate that the effect of IFN-γ is indirect (likely via activated macrophages), although exact mechanisms are yet to be elucidated (38). We have now included IFN-γ-induced apoptosis of T cells in the model.

Computer simulations

Our model is designed to represent the temporal immune response occurring dynamically in total lung. After deriving the model, we solve the nonlinear ordinary differential equation system to obtain temporal dynamics for each element of the model. For this purpose we use C code implementing the Runga-Kutta adaptive step-size solvers and appropriate finite difference methods. Finally, we validate our model output wherever possible with published experimental data.

As a marker of disease progression, we consider bacterial load as the most informative based on results from animal models (see a complete discussion of this in Refs. 13–15). We observe two stable states with the model: latent infection (controlled and low bacterial numbers) and active tuberculosis (uncontrolled bacterial growth). Reactivation is consequently defined as the transition from latency to active disease. Because latency is a stable state, it logically follows that reactivation can only occur due to perturbations to the system, e.g., waning immune response due to aging, HIV infection, malnutrition, or immunotherapy, etc. (e.g., TNF neutralization).

Because all parameters exhibit a range of values, it is important to note that a single simulation is not a unique representation of a certain state (latency or disease). Differential equation models yield as their output a representation of a sample average dependent on the parameter values used. Parameters may trade off to attain these states in a variety of ways and exhibit variable cellular/cytokine compositions for each of these states (see below).

Given the temporal nature of the model, we are unable to track lung physiology to study the extent and localization of tissue damage. We assess damage by measuring the effector cell (i.e., effector CD4$^+$ and CD8$^+$ T cell subsets) to target cell (infected macrophage (M_I)) ratio. A very large ratio would indicate greater tissue damage and vice versa.

All dynamics are plotted as described (linear or log scale), and all numbers indicate cell numbers/cytokine concentration per whole lung, but we consider the primary effector functions to occur within the context of the tuberculous granuloma. We have used available experimental and/or clinical data to establish parameters of our models. There are available data on cytokine concentrations in bronchoalveolar lavage fluid from human TB studies, although such data are not available from whole lung tissue in human TB. However, because TB is a disease that is primarily manifested in the parenchyma, we assume that our modeling space represents whole

lung. Additional data from mouse and nonhuman primate models of TB (Refs. 6, 10, and 40, and our unpublished data) have been incorporated where appropriate. All parameters are studied using a detailed uncertainty and sensitivity analysis (see below).

Deletion and depletion simulations

Simulations are performed mimicking in vivo experiments for the deletion of cells or effector molecules before infection (similar to a gene KO in a mouse model) and for the depletion of cells or effectors, where an element was removed from the system after latency had been achieved (day 500) (similar to Ab-mediated neutralization studies). Deletion experiments help us ascertain which elements of the system allow it to achieve latency, whereas depletion experiments help us understand which factors help maintain latency.

$CD8^+$ T cell kinetic studies

To explore the contributions of different subclasses of $CD8^+$ T cells on infection dynamics, we perform two experiments in which T8 and TC cells are differentially present, as suggested by Ref. 30. First, we allow only TC cells to be present for the first 200 days postinfection. Then we stop input of any further TC cells and allow those present to turn over naturally, based on their half-life. At that same day 200 time point we allow T8 cells to begin to develop, and they remain present until the end of the simulation. In another similar but opposite simulation we introduce T8 cells first, and then at day 200 postinfection we stop all further input of T8 cells and allow them to decay in two manners, fast or slow. At the same time point we allow TC cells to begin to develop, and they remain present until the end of the simulation. We track the effects to all model variables in the above simulations but only report the effects on total bacterial load.

Vaccine studies

To test what the model predicts about the effects of vaccination, we study four distinct scenarios. Each of these studies was performed with all parameters set to their latency values (Table III). First, we allow for only a class of $CD4^+$ Th1 memory effector cells to be present at the time of first challenge with Mtb. We simulate this by varying a given background level of memory cells that theoretically could be present in the lungs upon challenge. Second, we repeat the previous scenario by adding a background level of memory T8 cells while fixing the value of memory $CD4^+$ Th cells to a very small number that by itself would not lead to clearance. Third, we repeat this second scenario with TC cells rather than T8 cells. Values for memory cell levels used in each simulation are given in Table V. Finally, we include all three classes of memory cells in a number of simulations where we vary the levels of each subclass present to determine the effects of various combinations. In each of these simulations we assume that the input cells have a very long half-life, capturing their memory cell status. We track the effects of the presence of these memory cells for all model variables but only report them for total bacterial load.

Determining mechanisms that affect infection outcome

Rates measured from in vivo or in vitro studies likely vary with each repeated experiment due to inherent differences among hosts, even when using inbred mice, as well as to intrinsic errors of measurement. Further, some interactions in the Mtb-host system are not currently measurable. To explore the effects of uncertainty in the model, we evaluate all of the parameters using our own C code based on Latin hypercube sampling (41, 42). The Latin hypercube sampling method is a stratified Monte Carlo sampling mechanism that allows simultaneous, random, and evenly distributed sampling of each defined parameter that we contrast over a wide range. We vary each parameter by a factor of 1000 above and below reported literature data or mathematical estimates to assess the effects of parameter variations on model outcome (total bacterial load in this case). We combine the resulting uncertainty data with a sensitivity analysis using partial rank correlation to ascertain the sensitivity of the outcome variable (total bacterial load) against variations in parameter values. The Student's *t* test is then used to determine the significance of each partial rank correlation obtained, giving us a standard measure of sensitivity. Using these methods we are not only able to reveal key parameters that govern infection outcome but also able to evaluate temporal changes in the significance of these parameters as they relate to bacterial load. We provide only corresponding significance (p values) for brevity.

Control experiments

As a negative control the model simulates no infection, yielding an equilibrium value of resting macrophage population (3×10^5 cells), and all other variables are zero (infected and activated macrophages, all T cell subsets, and cytokines). If the innate response is up-regulated so that the initial macrophage interaction kills the bacteria, the model indicates that it is indeed possible to clear an initial low dose (<10 bacilli) infection without any memory of the response and no damage to the host (data not shown) (1).

Qualitative behavior of the previous model (15) is recapitulated by this updated model. Virtual IFN-γ and IL-12 deletion experimental results are in agreement with the outcomes reported in literature and also agree with those presented previously (15). We discuss TNF deletion and depletion elsewhere (S. Marino, D. Sud, J. Chan, J. L. Flynn, and D. E. Kirschner, manuscript in preparation). Recent availability of data on Mtb infection studies in humans and nonhuman primates (Refs. 43–49 and our unpublished data) have contributed to a more precise model of human infection.

Results

Simulating latent infection and active disease

The model simulates both infection outcomes of latent and active TB depending on the parameter values. As discussed previously (15), we used an extracellular bacterial load as a marker of disease progression, where uncontrolled growth of extracellular bacteria is indicative of active TB. These extracellular bacteria are derived in two ways: 1) from intracellular bacteria when infected macrophages are killed by CTL action or burst due to high bacterial load; and 2) from bacteria dividing in the extracellular spaces (at a slower rate than intracellular bacteria) (50–52).

Latent infection

The various cell and cytokine profiles associated with latency can be seen in Fig. 3. Extracellular bacterial load is extremely low (Fig. 3*A*) (<40 bacteria per whole lung), and all intracellular bacteria reside within a small number of chronically infected macrophages (Fig. 3*B*). The relationship between infected macrophages and intracellular bacterial numbers implies that during latency there are on average 50 bacteria within each of ~25 infected macrophages. Because some bacteria may be contained within resting and activated macrophages and thus quickly cleared, they are not included in this calculation. Resting macrophages maintain their numbers during latency due to the balance between their recruitment and subsequent activation or infection (Fig. 3*B*).

The $CD4^+$ T cell subset is composed mostly of Th0 cells, followed by Th1 cells and an extremely low level of Th2 cells (Fig. 3*C*). The total T cell population ($CD4^+$ and $CD8^+$ T cells combined) is comparable to numbers found experimentally (45). In this study we have assumed that the number of subclasses of $CD8^+$ T cells, namely T8 and TC, are equal in number with a 10% overlap in function. Later, we studied what happens when this ratio differs over the time course of infection. Here also, the T80 cells comprise most of the $CD8^+$ T cell population.

Simulated TNF levels are extremely low, because levels of infected and activated macrophages (the major TNF producers) are relatively low (Fig. 3*D*). This condition results in limited inflammation. Predicted ranges for IFN-γ and IL-10 correlate with studies measuring cytokine levels at the site of disease (47, 53, 54), whereas simulated IL-4 is present at essentially undetectable levels during latency (<0.1 pg/ml), possibly explaining why IL-4 is difficult to detect in humans with latent infection (54, 55). IL-12 levels in this particular latency simulation are higher than what might be found within the lungs, but this is likely due to the constraints of modeling within a single compartment, which means that priming of the T cell response occurs in the lungs instead of lymph nodes in this model. In other work from our group (14) involving a two-compartment system (lung and lymph node), IL-12 is higher in the lymphoid compartment.

Simulations indicate that latency is achieved by ~7–8 mo, and bacterial numbers are controlled (Fig. 3). Depending on certain parameter values associated with bacterial turnover and infection as well as cytokine production, these time points can be manipulated

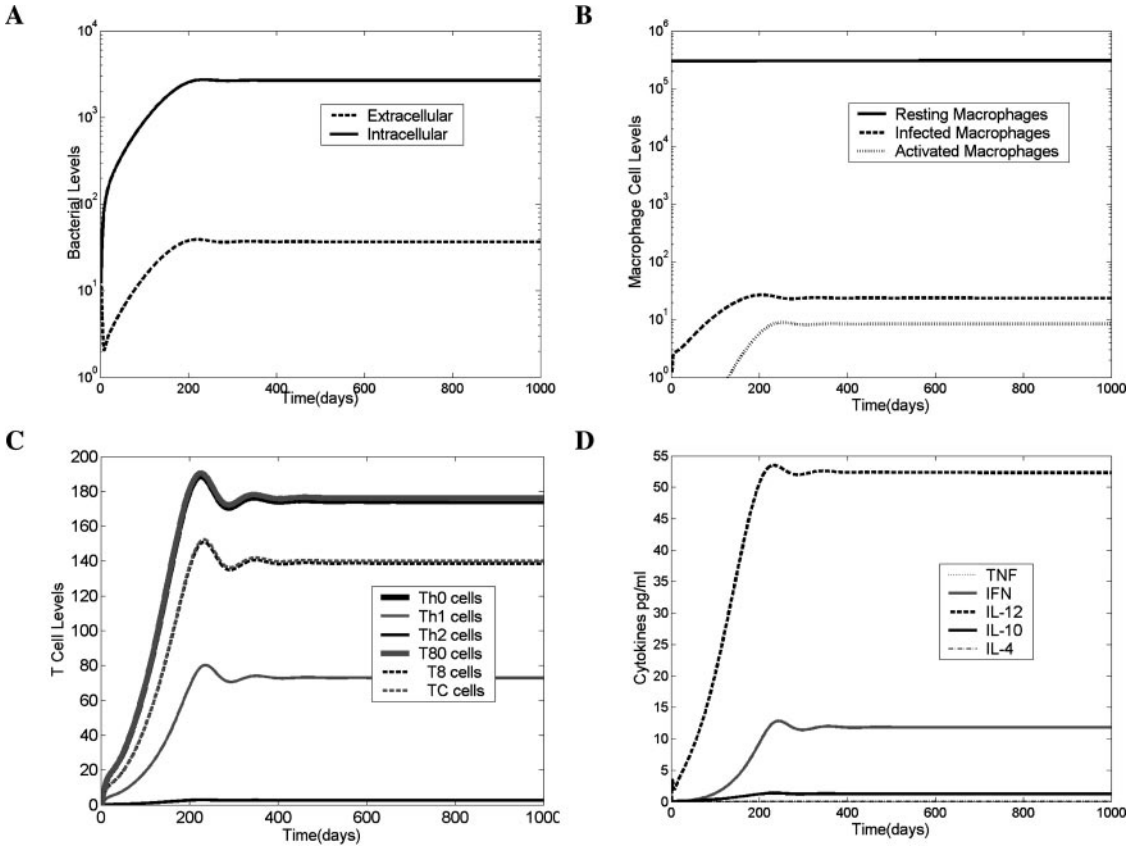

FIGURE 3. Simulations leading to latent infection. Shown are simulation results for all cells and cytokines in the model for the parameter values shown in Table III. Extracellular and intracellular bacterial populations are controlled by 200 days (*A*). Three subclasses of macrophages are shown (resting, infected, and activated) (*B*). All subclasses of T cells and cytokine dynamics are shown in *C* and *D*, respectively. Bacterial levels are controlled ~7–8 mo postinfection, and all model elements stabilize over time, indicating latency. The axes for bacterial and macrophage dynamics are given on a log scale. Units are total lung levels except for cytokine, which is expressed as picograms per milliliter.

to yield latent infection with different steady-state bacterial loads as well as cell and cytokine levels. Analysis of these parameters provides key insights into factors responsible for variations observed in patients infected with Mtb and also in regard to which parameters determine outcome. A subset of such parameters and their effect on the time to stabilized latent infection is shown in Table I.

Each of the parameters listed in Table I can affect the time to latency. This means that if the parameter shown increases, latency equilibrium is achieved much faster in all cases except for IL-4, where the opposite effect is observed. This is because IL-4 inhibits the development of a TH1 response, and this inhibition delays infection control.

Active tuberculosis

Only a subset of all model parameters can determine the infection outcome, i.e., latent infection or active tuberculosis. One other scenario that may occur under certain conditions is a system with oscillations, which is a less stable state than the latent state. This state allows for an enhanced chance of reactivation when any other small perturbation to the system is introduced. Our uncertainty and sensitivity analysis identifies which parameters have this property (Table II). By varying the parameters shown in Table II, the outcome is active tuberculosis rather than latent infection.

Plots for all model variables during active tuberculosis are shown in Fig. 4. Similar simulation results can be obtained varying any of the parameters in Table II; however, for this figure we reduced CTL activity (k_{52}). In contrast to the latent infection simulations (Fig. 3), here extracellular bacteria grow logarithmically (Fig. 4*A*). This result confirms that extracellular bacterial load is actually a marker of progression to disease. If most mycobacteria are contained within macrophages, then infection is being controlled; otherwise, bacteria continue to proliferate in extracellular spaces and disease ensues. The immune response does increase in response to infection but only up to a saturation limit, never succeeding to control infection.

Table I. *Parameters governing time to establishment of latent infection*

Parameter	Description	If Parameter Increases, Time to Latent Infection
α_{19}	Intracellular bacterial growth rate	Decreases
s_g	Extra production source of IFN-γ from NK cells	Decreases
μ_I	Loss of intracellular bacteria due to death of infected macrophages	Decreases
k_{17}	Rate of bursting of chronically infected macrophages	Decreases
α_{11}	IL-4 production by Th0 cells	Increases

Table II. *Parameters that affect Infection outcome*

Mechanism	Parameter Name[a]	Significance and Timing of Effect
IFN-γ production		
By NK cells	s_g (c_{10})	<0.01[b]
By CD4+ T cells	(c_{5a})	<0.001
By CD8+ T cells	α_{5b} (c_{5b})	<0.001
Macrophage activation		
Activation rate	k_3	<0.001
Strength of IFN-γ signal	(s_1)	<0.001
Strength of either TNF/LAM[c] signal	(c_8)	<0.01[d]
IL-12 production		
By dendritic cells	(c_{230})	<0.001
By macrophages	α_{23} (c_{23})	<0.001
Inhibitory effects		
IL-4 inhibition of IFN-γ action	(f_1)	<0.001[d]
IL-10 inhibition of IL-12 production	s	<0.05
Rate of IL-10 prod. by T cells	(α_{18})	<0.0001
Cytotoxicity		
Perforin/granulysin activity of CTLs	k_{52}	<0.001
Bacterial factors		
Intracellular growth rate	α_{19}	<0.001
Extracellular growth rate	α_{20}	<0.001
Rate of bursting of infected macs	k_{17}	<0.001[e]
Rate of phagocytosis	k_{18}	<0.05[d]

[a] Bacterial loads are increased or decreased significantly. Parameters in parentheses are positively correlated. Others are negatively correlated.
[b] First 50 days.
[c] Lipoarabinomannan.
[d] After 100 days.
[e] First 100 days.

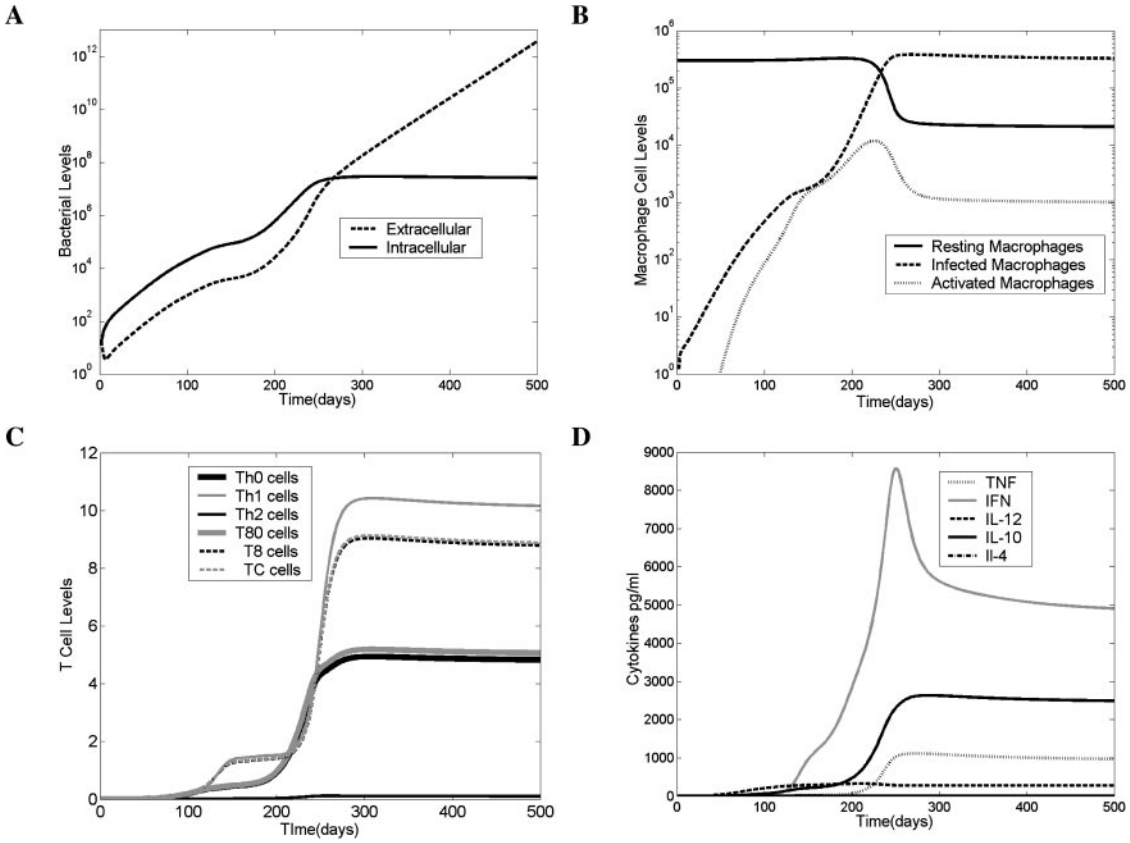

FIGURE 4. Simulations leading to active disease. Shown are simulation results for all cells and cytokines in the model for the parameter values shown in Table III; with one parameter different CTL activity is reduced (k_{52}). Bacterial population dynamics are shown in *A*. Note that, in contrast to Fig. 2, at 1 year postinfection the extracellular bacteria are growing logarithmically, whereas intracellular levels saturate infected macrophages. Macrophages are shown in *B*, and the level of infected macrophages has increased four orders of magnitude compared with latency. T cells and cytokines respond by increases in their numbers and concentration, but infection is not controlled (*C* and *D*). The axes for bacterial and T cell dynamics are indicated on a log scale, whereas macrophage and cytokines dynamics are specified on a linear scale. Units are total lung levels except for cytokine, which is expressed as picograms per milliliter.

Table III. *Estimated values for parameters*[a]

Parameter	Description	Range	Reference	Units
α_{5a}	IFN-γ production by Th1	1–100 (50)	Estimated	pg/Th1 day
α_{30}	TNF production by MI	1e-3–2e-2 (3e-3)	Estimated	pg/ml MI day
α_{5c}	IFN-γ production by MI	0.02–0.06 (0.03)	Estimated	pg/ml MI
α_{4a}	TNF-independent recruitment of MR	3e-3, 5e-3 (5e-3)	Estimated	1/day
α_{23}	IL-12 production by MR	1e-4–0.1 (2e-4)	Estimated	pg/ml MR
α_{5b}	IFN-γ production by T8 cells	1–100 (50)	Estimated	pg/T8 day
α_{18}	IL-10 production by TCs and T8s	2e-4–6e-2 (2e-2)	Estimated	pg/(CD8 total) day
α_{3a2}	Th2 recruitment by chemokines	0.001 (0.001)	Estimated	1/day
α_{3ac}	TNF-independent recruitment of TC/T8	9e-4, 1.45e-2 (3e-3)	Ref. 83 and estimated	1/day
α_{31}	TNF production by MA	0.3e-3–1.5e-2 (4e-3)	Estimated	pg/ml MA day
α_{1a}	TNF-independent recruitment of Th0	5e-3 (5e-3)	Ref. 83 and estimated	1/day
α_{32}	TNF production by Th1	8.16e-4 (8.16e-4)	Ref. 84	pg/ml Th1 day
α_{33}	TNF production by T8	0.6e-4, 1.1e-4 (0.6e-4)	Ref. 29	pg/ml T8 day
α_{3a}	TNF-independent recruitment of Th1	5e-3 (5e-3)	Ref. 83 and estimated	1/day
sr_{3b2}	TNF-dependent recruitment of Th2	1e3–1e5 (1e3)	Estimated	1/day
sr_{4b}	TNF-dependent recruitment of MR	1e3, 5e5 (2e4)	Estimated	MR/day
sr_{1b}	TNF-dependent recruitment of Th0	1e4–1e6 (2e5)	Ref. 83 and estimated	Th0/day
sr_{3b}	TNF-dependent recruitment of Th1	1e4–1e5 (2e4)	Ref. 83 and estimated	Th1/day
sr_{3bc}	TNF-dependent recruitment of TC/T8	1e3–8e4 (8e4)	Ref. 83 and estimated	T/day
f_9	Ratio adjustment, TNF/IL10	1–100 (50)	Estimated	Scalar
f_7	Effect of IL-10 on IFN-γ-induced Th0 to Th1	1 (1)	Estimated	Scalar
f_8	Ratio Adjustment, IL-10/TNF on MR recruitment	1,100 (1)	Ref. 85	
s_{4b1}	Half-sat, effect of TNF on Th1 recruitment	160–200 (165)	Estimated	pg/ml
s_{4b2}	Half-sat, effect of TNF on Th0 recruitment	100–500 (450)	Estimated	pg/ml
s_{4b}	Half-sat, TNF on MR recruitment	138, 556 (200)	Ref. 85	pg/ml day
β_2	Scaling factor of BT for TNF production by MA	1e-3, 1e-4 (1e-3)	Estimated	
β	Scaling factor of TNF for MR to MA	1e2–1e5 (1e2)	Estimated	BT/pg
c	Half-sat, IFN-γ on Th1 death	1067, 1173 (1100)	Ref. 86	pg/ml
c_c	Half-sat, IFN-γ on TC/T8 death	530, 600 (550)	Ref. 86	pg/ml
c_{52}	Half-sat, TC on MI killing	10–100 (50)	Estimated	TC
c_{T1}	Half-sat, effect of Th1 on TC cytotoxicity	1–1e4 (10)	Estimated	Th1
c_{5a}	Half-sat, MA on IFN-γ by Th1	5e3–2e4 (7e3)	Estimated	MA/ml
c_T	Half-sat, BT on TNF production by Th1/T8	1e3, 1e4 (1e4)	Estimated	BT
c_{5b}	Half-sat, MA on IFN-γ by T8	1e3–1e6 (7e3)	Estimated	MA/ml
c_{230}	Half-sat, BT on IL-12 by dendritic cells	1e3–1e5 (1e3)	Estimated	BT/ml
c_{23}	Half-sat, BT on IL-12 by MR	1e3–5e6 (5e3)	Estimated	BT/ml
c_4	Half-sat, (TC + Th1)/MI on MI apoptosis	20, 60 (40)	Ref. 87 and estimated	T/MI
w_3	Max percentage contribution by Th1 to Fas-FasL apoptosis of MI	0.4 (0.4)	Estimated	
w_2	Max, percentage contribution of MI-produced chemokines to MR recruitment	0.15 (0.15)	Estimated	
w_1	Max percentage contribution of Th1 to cytotoxicity	0.5 (0.5)	Estimated	
m	Percentage overlap between TC and T8 subsets	0.5–1 (0.6)	Estimated	Scalar
$\mu_{T\gamma}$	IFN-γ-induced apoptosis rate of Th1	1e-5–1e-3 (1e-4)	Ref. 86	1/MA day
$\mu_{Tc\gamma}$	Th1 IFN-γ-induced apoptosis rate of TC/T8	1e-5–1e-3 (1e-4)	Ref. 86	1/MA day
μ_{T8}	T8 death rate	0.33 (0.33)	Estimated	1/day
μ_{Tc}	Tc death rate	0.33 (0.33)	Estimated	1/day
μ_{T80}	T80 death rate	0.33 (0.33)	Estimated	1/day
μ_i	BI turnover to BE due to MI death, other mechanisms	0–0.005 (0.004)	Estimated	1/day
μ_{TNF}	TNF decay rate	1.112 (1.112)	Ref. 88	1/day
k_{14a}	Fas-FasL-induced apoptosis of MI	0.01–0.1 (0.1)	Estimated	1/day
k_{14b}	TNF induced apoptosis of MI	0.1–0.8 (0.1)	Estimated	1/day
k_{52}	Cytotoxic killing of MI	0.07–1 (0.5)	Estimated	1/day
s_{10}	Half-sat, IFN-γ on TNF production by MA	50–100 (80)	Estimated	pg/ml
s_{12}	Dendritic cell production of IL-12	200–1000 (300)	Estimated	pg/ml day
s	Describes IL-10 downregulation of IL-12 by MA	1–100 (10)	Estimated	pg/ml
δ_7	IL-10 production by MA	0.001–0.01 (0.01)	Estimated	pg/ml MA
N_{fraca}	Average no. of bacteria within a single MI released upon TNF-induced apoptosis	0.4–0.8 (0.5)	Estimated	Scalar
N_{fracc}	Average no. of bacteria within a single MI released upon Fas-FasL apoptosis	0.05–0.2 (0.1)	Estimated	Scalar
α_{20}	BE growth rate[b]	0–0.26 (0.05)		1/day
α_{19}	BI growth rate[b]	0.17–0.6 (0.4)		1/day
α_{12}	IL-4 production by Th2[b]	1e-3–9.1e-3 (1e-3)		pg/Th2 day
α_{11}	IL-4 production by Th0[b]	2.8e-4–4e-3 (5e-4)		pg/Th0 day
α_{17}	IL-10 production by Th2[b]	6e-4–6e-2 (6e-2)		pg/Th2 day
α_8	IL-12 production by MA[b]	8e–5 (8e-5)		pg/MA day
α_7	IFN-γ production by Th0[b]	0.02–0.06 (0.03)		pg/ml Th0
α_{16}	IL-10 production by Th1[b]	2e-4–1e-3 (2e-3)		pg/Th1 day

(*Continued*)

Table III. (*Continued*)

Parameter	Description	Range	Reference	Units
α_2	Max growth rate of Th0[b]	1e-4–2.8 (5e-3)		1/day
sr_m	MR recruitment rate[b]	600–1000 (1000)		MR/day
f_6	Adjustment, IFN-γ on IL-10[b]	0.025–0.053 (0.025)		Scalar
f_4	Adjustment, IL-10/IL-12 on IFN-γ[b]	0.76–3.2 (2)		Scalar
f_2	Adjustment, IFN-γ/IL-4[b]	0.0012–1.6 (1)		Scalar
f_1	Adjustment, IL-4/IFN-γ[b]	3–410 (200)		Scalar
s_2	Half-sat, IL-4[b]	1–10 (5)		pg/ml
s_6	Half-sat, IL-10 self-inhibition in MA[b]	51–60 (60)		pg/ml
s_4	Half-sat, IL-12 on IFN[b]	50–100 (50)		pg/ml
s_7	Half-sat, IL-12 on IFN-γ by NK cells[b]	5–100 (40)		pg/ml
s_1	Half-sat, IFN-γ on MR to MA[b]	50–110 (70)		pg/ml
s_8	Half-sat, IL-10 on MA deactivation[b]	1–1000 (1)		pg/ml
c_9	Half-sat, BE on MR infection[b]	1e6–1e7 (2e6)		BE
c_8	Half-sat, BT on MR activation[b]	5e4–5e5 (1e5)		BT/ml
c_4	Half-sat, T/MI ratio for MI lysis[b]	1–60 (40)		T/MI
c_{15}	Half-sat, MA on IFN-γ by Th1[b]	1e4–5e5 (2e5)		MA
c_{10}	Half-sat, bacteria on IFN by NK cells[b]	1e3–1e4 (1e3)		BT/ml
μ_{MR}	Death rate, MR[b]	0.0033 (0.0033)		1/day
μ_{MI}	MI death rate[b]	0.0011 (0.0011)		1/day
μ_{MA}	MA death rate[b]	0.07 (0.07)		1/day
$\mu_{i\gamma}$	IFN-γ decay rate[b]	2.16–33.2 (2.16)		1/day
μ_{i4}	IL-4 decay rate[b]	2.77 (2.77)		1/day
μ_{i10}	IL-10 decay rate[b]	3.7–7.23 (5)		1/day
μ_{i12}	IL-12 decay rate[b]	1.188 (1.188)		1/day
μ_{T2}	Th2 death rate[b]	0.33 (0.33)		1/day
μ_{T1}	Th1 death rate[b]	0.33 (0.330)		1/day
μ_{T0}	Th0 death rate[b]	0.33 (0.33)		1/day
k_2	MR infection rate[b]	0.2–0.4 (0.4)		1/day
k_3	MR activation rate[b]	0.2–0.4 (0.1)		1/day
k_{17}	Max. MI death due to BI[b]	0.02–0.8 (0.02)		1/day
k_4	MA deactivation by IL-10[b]	0.01–0.4 (0.08)		1/day
k_6	Max Th0 to Th1 rate[b]	2.9e-4, 5e-3 (5e-3)		ml/pg day
k_7	Max Th0 to Th2 rate[b]	0.02–0.7 (0.02)		ml/pg day
k_{18}	BE killing by MR[b]	1.2e-9–1.2e-8 (5e-9)		ml/MR day
k_{15}	BE killing by MA[b]	1.25e-7 (1.25e-7)		ml/MA day
s_g	IFN-γ production by NK cells[b]	0–1000 (100)		pg/ml day
N	Carrying capacity of infected macrophages[b]	10–100 (20)		BI/MI

[a] BE, extracellular bacteria; BI, intracellular bacteria; BT, total bacteria; Half-sat, half-saturation; MA, activated macrophages; MI, infected macrophages; MR, resting macrophages; T, naive T cells.

[b] Parameter that was estimated previously in Ref. 15.

Macrophage dynamics are shown in Fig. 4*B*. In the model, when a macrophage contains a threshold number of bacteria it bursts, releasing those bacteria to the extracellular environment where they can grow or be taken up by other macrophages. In progression to active TB, resting macrophages are depleted by an order of magnitude due to high levels of infection. Activated macrophage numbers increase and then fall off due to the following: 1) the short life span of activated macrophages; and 2) depletion of the resting macrophage pool due to infection (56). This transient rise in numbers indicates that severe tissue damage will occur (discussed below in the paragraph entitled *Measuring immunopathology*).

The total T cell population reaches a level comparable to that of the macrophage population (Fig. 4*C*). Because of the IFN-γ-induced apoptosis of Th1 cells, we observe a transient delay (before attaining peak values) that also correlates inversely with activated macrophage dynamics. This observation compares well with available experimental data regarding the necessity of activated macrophages for T cell apoptosis (37, 57, 58). $CD8^+$ T cell numbers are comparable to those of $CD4^+$ T cells and show dynamics most similar to those of Th1 cells due to IFN-γ induced apoptosis (Fig. 4*C*).

All cytokine levels are significantly elevated during disease. TNF levels are increased by several orders of magnitude to >1000 pg/ml (Fig. 4*D*), which has been associated with severe pathology (59). Other cytokine levels correlate with experimental data (47, 60). In unpublished data from our nonhuman primate studies with active TB, $CD4^+$ and $CD8^+$ T cell production of IFN-γ increases substantially compared with that of latently infected monkeys. In addition, there is an increase in $CD4^+$ and $CD8^+$ T cells in the lungs of mice with fulminant TB compared with controlled infection (61) (our unpublished data).

Factors that determine infection outcome

The model consists of >100 parameters that govern rates and interactions between various components that can differ among individuals and potentially can affect progression to active tuberculosis or to latent infection (see Table III and *Appendix*). Varying each of these parameters over a large range simultaneously to perform sensitivity analyses demonstrates that changes in only a small subset of parameters are influential in distinguishing between infection outcomes (Table II). Logically, a tradeoff exists between these parameters; changing a parameter toward more stringent control can be compensated for by varying another to aggravate infection with no resulting change in outcome. For example, an increased extracellular bacterial reproduction rate (α_{20}) can be controlled by increasing the rate of CTL activity (k_{52}).

IFN-γ is an important cytokine for macrophage activation and, not surprisingly, is relevant in determining infection outcome (Table II). The rate of production of IFN-γ from all three sources ($CD4^+$ and $CD8^+$ T cells and NK cells) has a positive effect on

control of infection. However, the contribution of NK cells is particularly important in the initial phases of the infection ($p < 0.01$ for the first 50 days), whereas the contribution from T cells is important throughout the infection ($p < 0.001$). Related to the findings with respect to IFN-γ production, cytokine parameters that control the rate of macrophage activation (IFN-γ and TNF) determine the outcome of infection as well, with increased macrophage activation promoting establishment of latency. Parameters that influence IL-12 production by macrophages and dendritic cells (c_{23}, α_{23}, and c_{230}) and, therefore, the robustness of the type 1 response, can determine the outcome of infection and are important throughout the course of infection. Along these same lines, those parameters that inhibit a type 1 (IFN-γ producing) T cell response, such as IL-4 inhibition of IFN-γ effects (f_1) and IL-10 mediated inhibition of IL-12 production (s), have a negative effect on the establishment of latency. Increasing the rate of production of IL-10 from T cells (α_{18}) results in progression to disease due to multiple effects of this cytokine, including inhibition of macrophage activation, IFN-γ production, and TNF-mediated apoptosis.

In addition to the IFN-γ production by CD8$^+$ T cells, a parameter (k_{52}) that governs the perforin/granulysin-mediated cytotoxicity of infected macrophages with the subsequent killing of intracellular bacteria influences infection outcome. Decreasing the rate of these killing mechanisms leads to disease.

Bacterial factors that determine infection outcome include both the intracellular (α_{19}) and extracellular (α_{20}) bacterial replication rates, the ability of bacteria to be taken up into macrophages and destroyed by phagocytosis (k_{18}), the rate of bursting of infected macrophages due to bacterial overload (k_{17}), and the turnover of bacteria from intracellular to extracellular due to natural death of infected macrophages (μ_I) (Table II). This suggests that certain bacterial factors that are strain dependent can influence infection outcome. In particular, factors in the model that increase the extracellular bacterial load are all influential in infection outcome. Also suggested from these data is the idea that the growth rate inside macrophages, as well as perhaps cell wall factors that affect phagocytosis, should influence the ability of a strain to cause disease. This possibility is supported by literature comparing the virulence of different clinical strains of bacteria (62–64).

Recruitment of cells to the site of infection is clearly relevant to control of infection. Based on our previous data in animal models (33), we include both TNF-dependent and independent recruitment terms. There are several recruitment parameters in the model that are crucial in determining infection outcome (data not shown). Interestingly, those parameters that are most important are TNF-dependent. A full discussion of the predicted roles of TNF in TB from this mathematical model is the subject of another manuscript (S. Marino, D. Sud, J. Chan, J. L. Flynn, and D. E. Kirschner, manuscript in preparation).

Measuring immunopathology

Because we do not specifically track the lung tissue environment where infection is occurring, we define tissue damage based on the ratio of effector T cells to infected macrophages (see *Materials and Methods*). In other work (65) we focused on granuloma formation, examining the spatial aspects of infection together with the development of necrosis. An overexuberant immune response can lead to tissue damage, including necrosis. Caseous necrosis within a granuloma may actually contribute to control of infection (66), perhaps by creating anoxic (anaerobic) conditions (our unpublished data). In this work we specifically address the contribution of TNF and CD8$^+$ T cells to immunopathology. Presented in Table IV are those factors that play a role in tissue damage, including those identified in our previous work (15). The model predicts that increased TNF production beyond a threshold level results in a high effector T cell to infected macrophage ratio, thereby causing tissue damage.

Inhibition of macrophage/T cell recruitment by IL-10 is important for controlling immunopathology. Modulation of T cell numbers within the lungs also influences pathology. An important mechanism that controls T cell numbers in mycobacterial infection is IFN-γ-induced apoptosis, which may prevent excessive activation of resting macrophages and the resulting tissue damage (37). The model indicates that decreased T cell apoptosis results in improved control of infection, but with a cost of increased tissue damage ($\mu_{Tc;}$ Table IV). Such delicate balances emphasize the tradeoff between tissue-damaging responses and important down-regulatory mechanisms, as suggested by others (66).

Cytokine dynamics

Shown in Fig. 5 are the infection outcomes following deletion (Fig. 5*A*) and depletion (Fig. 5*B*) for four key cytokines in the model. Note that TNF deletion or depletion results by far in the fastest progression to disease as compared with deletion of IL-12 or IFN-γ. IL-12 and IFN-γ deletion simulations both approach disease with similar kinetics, and IL-10 deletion is only slightly different from that of the latency control. Results are consistent across deletion and depletion studies, indicating that those cytokines that are important in establishment of latency are also relevant for maintaining the infection in a latent state.

T cell contributions to immunity

Our updated model is consistent with experimental data predicting that key immune components responsible for controlling initial and latent Mtb infection are CD8$^+$ CTL activity and IFN-γ production (4, 30, 67–69). Cytotoxic activity of CD8$^+$ T cells accounts for ~80–90% of the killing of infected macrophages and up to 80% of the granulysin-mediated killing of bacteria within those macrophages; this activity is crucial to control of infection

Table IV. *Parameters affecting immunopathology*

Parameter	Description	Increased Damage Occurs When Value Is[a]
α_{30}	TNF production rate by MI	Increased
δ_7	IL-10 production rate by MI	Decreased
sr_{3bc}	TNF-dependent recruitment rate of TC and T8	Increased
α_{11}	IL-4 production rate by Th0	Decreased
f_8	Extent of inhibition of macrophage recruitment by IL-10	Decreased
μ_{Tc}	IFNγ-induced apoptosis rate of Th1	Decreased
k_{52}	Rate of cytotoxic killing of MI by TC	Increased
μ_{TNF}	Decay rate of TNF	Decreased

[a] Compared to values used to generate latent infection simulation (Table III).

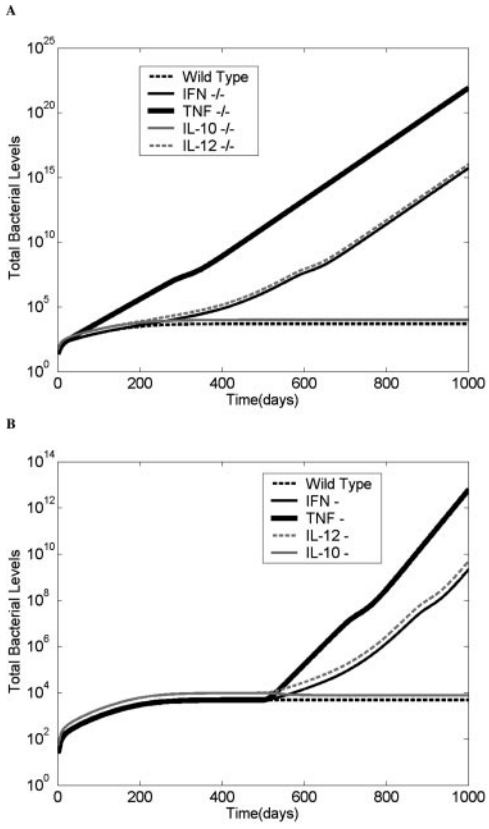

FIGURE 5. Cytokine deletion and depletion. Shown are the simulation dynamics of total bacteria levels during deletion (indicated by $-/-$) (*A*) and depletion (indicated by $-$) (*B*). Deletions and depletions were performed for IFN-γ (thin, dark, solid lines), TNF (thick, dark, solid lines), IL-12 (gray dashed lines), and IL-10 (gray solid lines). Deletions imply that a cytokine was removed from the system at day 0, whereas for deletion it is removed at day 500. Simulations are shown compared with latency (wild type; dark dashed lines) as a positive control.

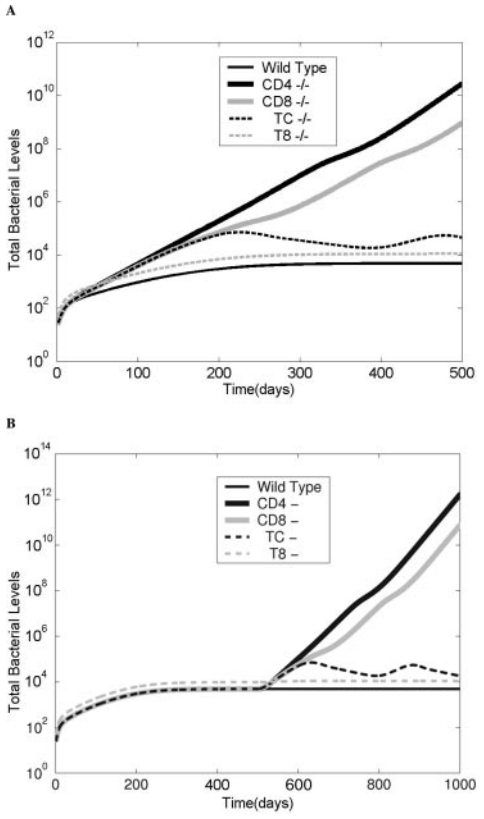

FIGURE 6. T cell deletion and depletion. Simulations of total bacterial dynamics are shown for deletion (indicated by $-/-$) (*A*) and depletion (indicated by $-$) (*B*) simulations. For deletions, T cells were removed from the system at day 0. For depletions, cells were removed at day 500 after the system has achieved latency. Deletion and depletion simulations were performed for total $CD4^+$ T cells, total $CD8^+$ T cells, T8 cells, and TC cells. These were compared with latency (wild type) as a positive control.

($k_{52;}$ Table II). The Fas-FasL apoptosis of infected macrophages induced by $CD8^+$ T cells also appears to be important early in infection, in contrast to published in vitro studies (26, 70) that examined the effects of this pathway on killing intracellular mycobacteria.

T cell deletion studies

The updated model reflects the contribution of all of the major T cell subsets, which allows us to analyze the importance of each subset at different times in infection. Fig. 6 presents deletion (Fig. 6*A*) and depletion (Fig. 6*B*) simulations of various T cell population subsets. As stated previously, deletion simulates the loss of a component from the beginning of infection (similar to a KO mouse). Depletion studies simulate loss of a component during a latent infection (500 days postinfection), similar to Ab-mediated depletion or neutralization of cells or cytokines. Depletion studies closely match the deletion results (compare Fig. 6, *A* and *B*), supporting the hypothesis that similar factors are important for controlling both initial and latent infection.

Simulations in which either total $CD4^+$ or $CD8^+$ T cell populations are deleted always result in disease. Disease (as marked by total lung bacterial load) develops more slowly when $CD8^+$ T cells are deleted as compared with $CD4^+$ T cell deletion (Fig. 6), which is consistent with experimental studies (12). In the $CD8^+$ T cell deletion simulation, overall cell numbers are maintained as increased macrophage numbers compensate for a decline in $CD8^+$ T cell numbers, and CTL killing of infected macrophages is greatly reduced (data not shown). All cytokine levels are similar to those observed during disease (Fig. 4), which is in agreement with published data (20) on IFN-γ and TNF production in mice without $CD8^+$ T cells.

Selective T8 or TC deletion

We exploit the model to specifically delete either T8 or TC subsets at day 0 to determine the relative contribution of each to control of infection. The resulting bacterial loads from selective T8 and TC deletion are shown in Fig. 6*A*. For T8 deletion, latent infection is achieved, although bacterial numbers are slightly higher than the standard latent infection values (wild type). In the absence of T8 cells, IFN-γ production by CD4 T cells (Th1) and NK cells increases to maintain total levels of IFN-γ (data not shown).

For TC deletion, latent infection is achieved; however, bacterial loads are an order of magnitude higher, and oscillations appear. The presence of oscillations in total bacterial numbers indicates a less stable state of latency. This result suggests that an additional, even minor, perturbation of the system could result in reactivation, whereas the same perturbation in the presence of TC cells would not affect the latency state. To test this hypothesis, an experiment was performed in which TC cells were deleted and the rate of IL-10 production by Th1 was increased (over a range of values) compared with the standard latency values. In this case, the outcome was always uncontrolled bacterial growth (data not shown). Varying the IL-10 values over the same range in the presence of TC cells (normal latency levels) did not affect the outcome of infection.

An unexpected result of the CD8$^+$ T cell subset deletion simulations was the apparent synergy between these subsets that is important in the immune response to Mtb. When both T cell subsets were removed simultaneously, the system was driven to active disease. However, when T8 and TC were removed individually, latency was still achieved, but at a cost to either bacterial numbers or system stability, respectively. Taken together, these deletion and depletion studies support the view that T8 and TC cell subsets act in synergy to control infection.

T cell depletion

To explore the role of T cells in maintaining a latent infection, we performed depletions by removing CD4$^+$ and CD8$^+$ T cells as well as both functional subsets (T8 and TC cells) from our system at 500 days postinfection (while the system is in latency). Fig. 6*B* illustrates the dynamics of the total bacterial population in the lungs during latency (<500 days), depletion, and subsequent advancement to disease (>500 days). The results match those of the deletion cases (Fig. 6*A*). This finding implies that T cells are crucial in both establishing as well as maintaining latent infection.

CD8$^+$ T cell subsets: dynamic changes during the course of infection

Experimental data from a C57BL/6 mouse model suggest that the functions of CD8$^+$ T cells are differentially regulated during infection (30). Cytotoxic function was observed only during the

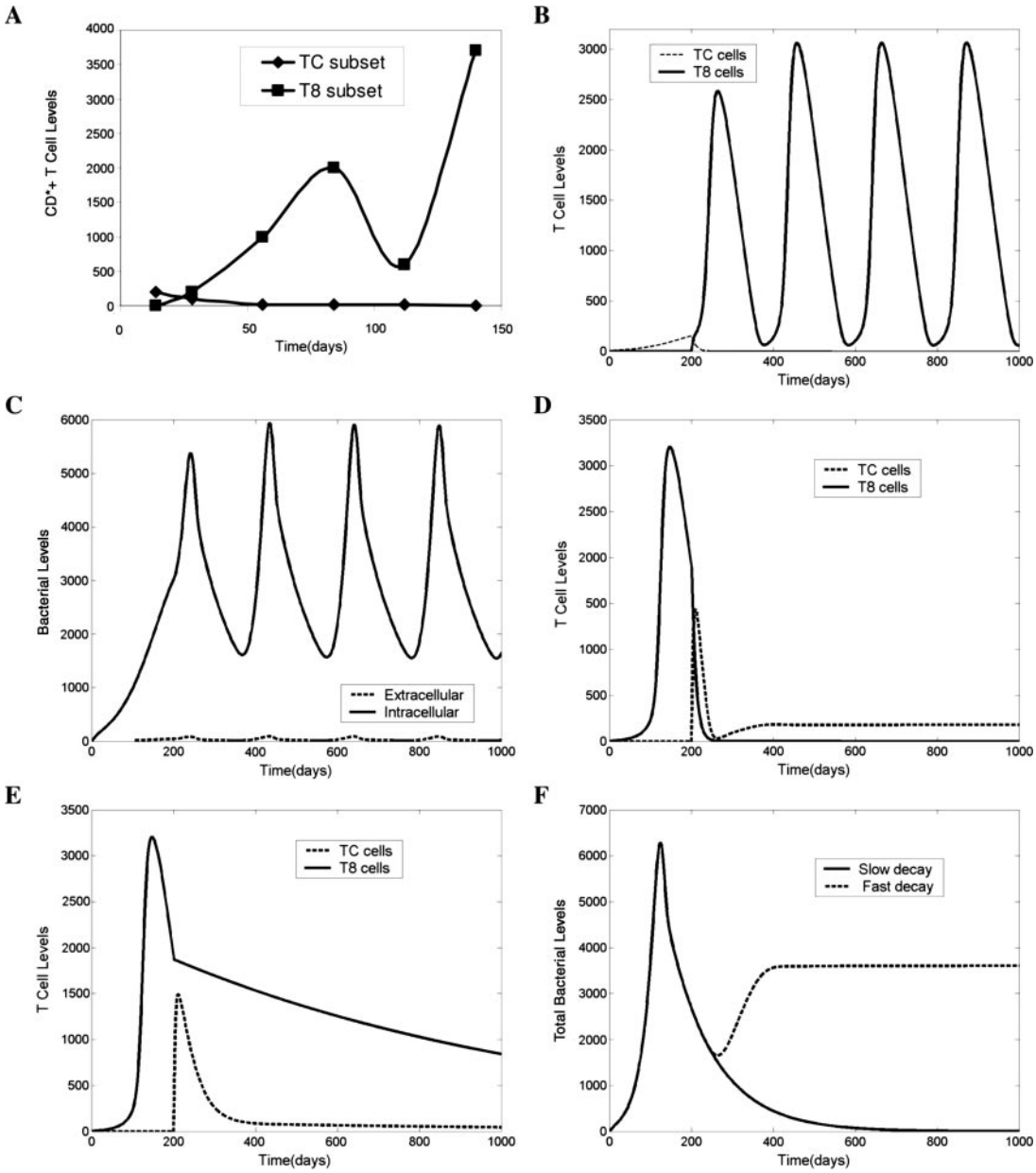

FIGURE 7. CD8$^+$ T cell kinetic studies. *A*, Data from Ref. 30 indicating the differential presence of T8 and TC populations a mouse model of TB. The progression time frame for a murine model is likely faster than that observed in humans. *B–F*, Simulations exploring the timing of CD8$^+$ T cell kinetics. *B*, Dynamics of two subsets of CD8$^+$ T cells when TC cells are present first and then, at the 200 day time point, they die off naturally and T8 cells are introduced and are allowed to increase. *C*, The corresponding bacterial subpopulations. Notice that oscillations are now present in the system as compared with latency (Fig. 3*A*). *D* and *E*, The opposite orientation, where T8 cells are present first for 200 days and are allowed to die off either fast (*D*) or slow (*E*) while the TC cell subset replaces the T8 cell subset. *F*, total bacterial dynamics during the fast (dashed line) and slow (solid line) T cell dynamics from *D* and *E*, respectively.

initial phase of infection, whereas IFN-γ production by $CD8^+$ T cells did not occur until the chronic phase of infection (see Fig. 7*A*, adapted from Ref. 30). Until now, we assumed that the total $CD8^+$ T cell population was comprised of equal numbers of T8 and TC cell subsets. We can now vary this assumption to test the experimental predictions of Lazarevic et al (30). In the murine system, the dynamics of infection occur on a faster time scale than that of humans and nonhuman primates. In the studies of Lazarevic et al. (30), the observed a switch in $CD8^+$ T cell phenotype in < 50 days. In the simulations in this study, we allowed the system to evolve further for 200 days (just into the latent state; see Fig. 3) before we induced a switch. We first simulated the situation described in Lazarevic et al. (30) in which TC cells existed exclusively for 200 days and, as they declined, we introduced IFN-γ-producing activity via T8 cells in an increasing and also exclusive fashion (Fig. 7*B*). In this case, the system no longer approaches latency as a steady state but instead reveals oscillations in bacterial numbers (Fig. 7*C*), suggesting a less stable latent state. Further, the average levels of bacteria during the course of infection in this simulation are higher than when both subclasses of $CD8^+$ T cells are present throughout infection.

It is possible that this naturally occurring order of effector T cell dominance scenario (TC cells first, then T8 cells) may not be the most effective in controlling infection. To address this question, we compared the effects of opposite differential timing of $CD8^+$ T cell function on the outcome of infection (Fig. 7, *D* and *E*) when IFN-γ producing activity is introduced first and exclusively followed by cytotoxic activity. This was done in two ways: first, a rapid decline in T8 cells (to zero from 180 to 220 days) while TC cells were increasing (beginning at 200 days) (Fig. 7*D*) and, second, where the decline in T8 cells was very slow (over a period of >1000 days) (Fig. 7*E*). In both simulations, total bacterial numbers increased dramatically during the first 100 days of infection and then were controlled (Fig. 7*F*). In the situation where T8 cells declined quickly a latent state was achieved at, however, a higher bacterial level than normal latency levels (compare Figs. 7*F* and 3*A*). In contrast, when T8 cell levels decreased very slowly, the infection was actually cleared. We interpret this to mean that modestly increased bacterial numbers during the initiation of an immune response, caused by a lack of TC cells, enhances the overall induction of an immune response (by having more Ag driving stronger T cell responses). When T8 cells are declining slowly and TC cells enter the lung, the stronger immune response can clear infection. In contrast, if T8 cells are not maintained, TC cells are sufficient to control infection (when TH1 cells are also present), but at a slightly higher bacterial load. Thus, a T8 cell to TC cell switch has

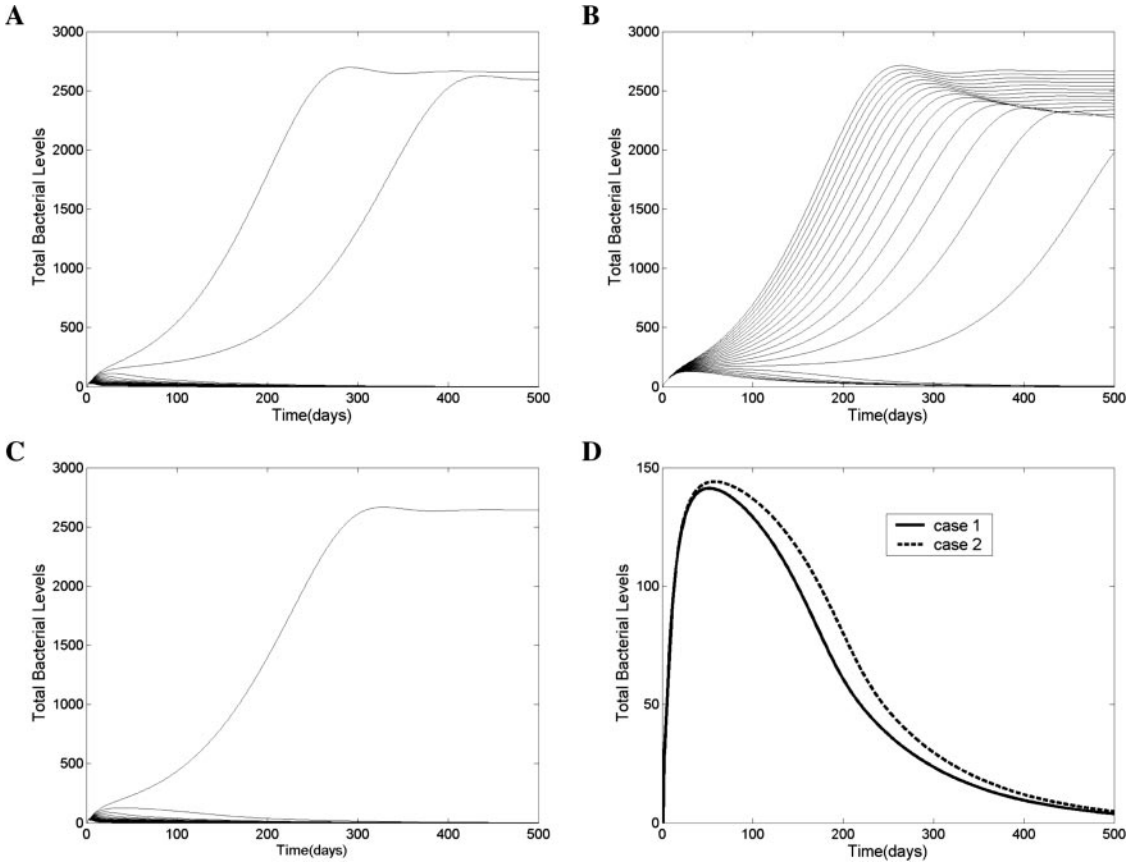

FIGURE 8. Vaccine strategies. In these simulations we test the effects of a cell-mediated vaccine by exploring the presence of different T cell subsets on infection progression. We vary the number of T cells of each subset in each simulation for 20 different values over a wide range (using the Latin hypercube sampling algorithm; see *Materials and Methods*) and show results for total bacterial loads. In *A* we show the total bacterial load when a range of Th1 cells are present at the time of infection at the site (values are shown in the left column of Table V). Of the 20 different values for numbers of Th1 cells (over a range of 1–35), only two did not lead to clearance (1 and 3). In *B* we set the level of Th1 cells to 3 and then input a range of T8 cells (values in the middle column of Table V range from 1 to 150). In this case, clearance of bacterial challenge is only possible when there are a great number of T8 cells present (>75). In *C* we set the levels of Th1 cells to 3 and then input a range of TC cells (values in the right column of Table V range from 1 to 150). Here, all but the lowest case (two TC cells) can lead to clearance. In *D* we input all three subsets (Th1, and T8, and TC) in two different combinations: case 1 presents three Th1 cells, two T8 cells, and three TC cells. Case 2 presents three Th1 cells, no T8 cells, and three TC cells.

an improved outcome compared with what might be the natural situation of TC cell to T8 cell switch, as observed by Lazarevic et al. (30). This improvement, however, comes at the expense of a 12% increase in levels of damage (as measured in our model by effector to target cell ratios) over the first 50 days after the switch.

Vaccine strategies

Given the prevalence of Mtb worldwide, a clear need exists for an effective vaccine strategy to impart protective immunity against TB. Bacillus Calmette-Guérin, the vaccine against TB used for the last 80 years, has failed to control the TB scourge (71). Much of TB vaccine development has been empirical, because mechanisms of resistance to TB are incompletely understood. Using the model generated here, we address possible strategies that target different T cell subsets with the goal of illuminating vaccine approaches that will lead to the best control of infection.

Initially, we investigated the ability of single T cell subsets to provide protective immunity, assuming that effector memory cells of that phenotype were present in the lungs, poised to respond immediately to a challenge. When memory Th1 cells alone were present at levels of 10% of their peak values that lead to latency (Fig. 2; see 200 days postinfection), clearance of the challenge infection was observed (Fig. 8*A* and Table V). Similarly, when memory TC cells were present at 10% of the peak value of latency values (Fig. 2) (plus a few Th1 cells present that would be insufficient to clear the challenge; see Fig. 8*A*), clearance of challenge infection was observed (Fig. 8*B* and Table V). Conversely, if the memory response present at challenge was T8 cells (plus the same small number of Th1 cells as in the TC memory scenario), a large number of these cells (~75% of peak values from latency) were necessary to observe clearance (Fig. 8*C* and Table V).

Memory responses that are a combination of TC, T8, and Th1 can lead to clearance of infection at substantially lower numbers of each type of cell (Fig. 8*D*). We performed uncertainty and sensitivity analyses on levels of memory cells present at the time of challenge. Th1 and TC cells are highly negatively correlated ($p < 0.0001$) with total bacterial load. T8 cells are also negatively correlated with total bacterial load, but to a lesser degree ($p < 0.01$). Using the uncertainty and sensitivity analysis (see *Materials and Methods*), we estimated that 4% of peak Th1 cells and 2% of peak TC cells together are the minimum numbers that are required to be present as effector memory cells in the lungs for clearance of a challenge (Fig. 8*D*). This result is independent of memory T8 cell numbers. However, if T8 memory is present at very high levels (~35% of peak T8 values), the numbers of Th1 and TC can be reduced (data not shown). In practice, such high T8 effector memory cell numbers would be very difficult to obtain and maintain in the lungs by vaccination.

From these data we hypothesize that induction of moderate Th1 and TC subsets should be sufficient as a vaccine against challenge, although retaining these cells in the lungs as effector memory cells is crucial to obtaining this outcome. In fact, if the memory cells do not arrive in the lungs within the first 3 days of infection, clearance is not observed (data not shown). The approach that could achieve this result may be related to mucosal routes of vaccination. In practice, it is not obvious how to vaccinate to modulate TC levels specifically, and, most likely, moderate levels of TC and T8 would be induced in any CD8-directed vaccine approach. Second, the percentages of T cells presented should be viewed simply as guidelines rather than as absolute numbers of cells that must be present, because these may be dependent on the genetic susceptibility of a particular person. Targeting both CD4$^+$ and CD8$^+$ T cell subsets will be the most efficient strategy for an effective vaccine, but a high peak response to the vaccine might be necessary to retain reasonable levels of these cells as effector memory cells in the lungs.

Table V. *Values for T cell subsets present in vaccine study*

Th1 cells	T8 cells	TC cells
1.85	4.725	4.725
3.55	12.175	12.175
5.25	19.625	19.625
6.95	27.075	27.075
8.65	34.525	34.525
10.35	41.375	41.375
12.05	49.425	49.425
13.75	56.875	56.875
15.45	64.325	64.325
17.15	71.775	71.775
18.85	79.225	79.225
20.55	86.675	86.675
22.25	94.125	94.125
23.95	101.575	101.575
25.65	109.025	109.625
27.35	116.425	116.475
29.05	123.925	123.925
30.75	131.375	131.375
32.45	138.825	138.825
34.15	146.275	146.275

[a] In the left column, only Th1 cells are present. In the middle column, three Th1 cells are present together with the indicated number of T8 cells. In the right column, three Th1 cells are present together with the indicated number of TC cells.

Discussion

In this study we extended our previous work in modeling the immune response to Mtb to examine the role of CD8$^+$ T cells in the course of Mtb infection in humans. CD8$^+$ T cell numbers were tracked in the course of infection, and we also incorporated both their cytokine-producing and CTL function. The model can easily simulate all possible infection outcomes: clearance, latency, disease, and reactivation. Clearance is achievable via an enhanced innate response or persistent activated macrophage action. We were able to ascertain critical parameters that govern infection outcome between latency and disease (Table II) and also determine parameters that control the time profile of these outcomes. Reactivation can be achieved by varying the parameters specified in Table II toward disease either slowly (representing aging or slow loss of immune function) or quickly (representing immunosuppressive therapy). Disease outcomes can be simulated for wild-type scenarios as well as for individuals with impaired macrophage (lower numbers) and/or impaired T cell responses. Tighter control of bacterial numbers may be achieved at the expense of tissue damage induced by excessive TNF production and a vigorous CTL response.

The data from these simulations strongly support the hypothesis that although IFN-γ is necessary for a protective immune response to Mtb, it is not sufficient. These results are supported, for example, by murine studies of acute and chronic infection of CD4$^+$ T cell-deficient mice in which CD8$^+$ T cells produced enough IFN-γ to match wild type levels in lung, yet the mice still succumbed to the infection (40, 72, 73). The data also support the belief that CD4$^+$ T cells are very important for control of infection, as is generally accepted in the field, but highlight the finding that the contribution of CD4$^+$ T cells to the control of Mtb infection is more than just production of IFN-γ. This can be most easily observed by comparing the CD4$^+$ T cell and IFN-γ deletion or depletion scenarios (Figs. 5 and 6), where loss of CD4$^+$ T cells is

more detrimental in terms of time to active disease than loss of IFN-γ.

A consistent theme observed in all simulations performed was that mechanisms important in controlling initial infection also contributed to the maintenance of latent infection. This observation is supported by some (4–6, 40, 72–76) but not all (77) experimental findings in the literature. These results further suggest that there is continual need for dynamic control of infection rather than a special state attributed to latent infection. In the simulations where we study the mechanisms yielding different infection outcomes (using the uncertainty and sensitivity analysis), the values for all cells and cytokines adjust their levels slightly, yielding myriad different routes to latency or active disease for each combination of parameters. This variation could account for differences among individuals (and possibly between animals and humans) in response to infection and suggests that levels of effector cells and molecules necessary for achieving and maintaining latency may differ.

Using the updated model, we were able to assess the contributions of the various T cell subsets to the control of Mtb, both in the setting of natural infection and in a vaccinated individual. $CD8^+$ T cells have at least two major functions that are important in control of Mtb infection: 1) cytotoxic activity, which can result in intracellular bacterial killing as well as killing of the infected macrophage; and 2) cytokine production. In this study we defined two subsets, TC (cytotoxic $CD8^+$ T cells) and T8 (IFN-γ producing $CD8^+$ T cells), based on literature indicating that these two subsets may be differentially regulated (1, 5, 6). This provided the opportunity to determine the contribution of each subset to control of infection. Although no human or primate TB data for such deletion/depletion experiments are available, we were able to compare our results to murine experiments involving T cell depletion via Ab treatment, as well as genetic KOs resulting in dysfunctional $CD8^+$ T cells (12, 20, 78). However, in the mouse model it is technically challenging or impossible to selectively deplete either cytotoxic or IFN-γ producing subsets during chronic infection. In addition, KO mice can have dysregulated immune responses that prevent accurate analysis of the exclusive effects of the mutation. For example, we and others (9, 79) demonstrated previously that perforin KO mice (i.e., with $CD8^+$ T cells impaired in cytotoxic potential) had dysregulated IFN-γ production (up to 4-fold higher) during Mtb infection, making it impossible to determine the true contribution of CTL to the control of the infection. In contrast, mathematical models are not subject to these complications. Finally, mice are lacking in what appears to be a crucial factor, granulysin, in the ability of $CD8^+$ T cells to control Mtb infection. Using the mathematical model, we were able to include granulysin action in the CTL subset and directly study the effects of the actions of this molecule in the immune response to Mtb.

Our findings indicate that both subclasses of $CD8^+$ T cells can play a role in the immune response to Mtb. Deletion or depletion of either subset can still allow the host to control the infection, but either total bacterial numbers during latency are slightly higher (in the case of absence of T8 cells) or total bacterial numbers oscillate (in the case of loss of TC), indicating a less stable latent state. The less stable latent state is more susceptible to minor perturbations, and small changes can lead to reactivation in this setting (data not shown). However, given the data regarding removal of a single $CD8^+$ T cell subset, the surprising finding is that removal of both $CD8^+$ T cell subsets together always results in active disease, suggesting that some contribution from either $CD8^+$ T cell subset is necessary to control infection.

This model was used to explore the timing of $CD8^+$ T cell effector functions. In the literature, Ag load or extent of priming in viral infections has been postulated to influence $CD8^+$ T cell effector functions, with higher Ag load leading to a more cytokine-producing phenotype. Our group has published data (30) suggesting that, early in infection (in C57BL/6 mice), cytotoxic activity but little IFN-γ production from $CD8^+$ T cells is observed in the lungs. When infection reaches the chronic stage there is a buildup of Ag in the lungs, and the $CD8^+$ T cell phenotype appears to switch to IFN-γ production. Using the model, we compared the scenarios of first initiating TC function followed by T8 function (the naturally occurring situation) with the opposite orientation, i.e., T8 cells appearing first and then switching to TC cell function. In the first scenario (the early appearance and then decline of TC cells, with T8 cells appearing later in infection), the system could reach latency but with a higher and oscillating bacterial load (i.e., a less stable latent state). In contrast, if T8 cells were present initially but declined quickly as TC cells were introduced into the system, a stable latency was achieved. Furthermore, if the T8 cells were declining more slowly during the introduction of TC cells, clearance of the infection was achieved. This was the result of a higher bacterial load during the initiation of the response (caused by a lack of TC cells) and a stronger T cell response induced by increased Ag load in the system. This outcome was recapitulated by removing Th1 cells from the intact system for the first 100 days and then adding them back; this scenario also led to clearance due to higher total bacterial numbers (and Ag) during the priming phase of the response. These results confirm the importance of the TC subset in the control of infection but also suggest that a higher amount of Ag (perhaps more bacteria) in the system initially might lead to a stronger response and better protection against disease. The results further suggest that the low ID_{50} of Mtb may serve as a key virulence strategy.

The updated model lends itself to the study of mechanisms of vaccine-induced protection. Vaccine development for TB has been mostly empirical because little is known about the protective mechanisms for this disease, and there are no useful surrogate markers of protection. In this work, we sought to define the requirements for protective vaccination against Mtb infection based on a T cell-mediated immune response. The model allows one to create scenarios that are impossible in animal models or human systems to elucidate key elements of protection. We identified the minimum level of memory TH1, T8, or TC cells that would be necessary to obtain clearance of a challenge infection. For Th1 alone or TC alone (with a small number of Th1 cells), effector memory populations at levels of ~10% of the peak values (~200 days in the latency scenario) would need to be maintained in the lungs to offer protection. In contrast, enormous numbers of memory T8 cells (75% of peak initial expansion) would need to be present in the lungs at time of challenge to lead to clearance. A combination of moderate levels of memory Th1 and TC cells were much more effective in achieving protection against challenge. In this situation, the minimum memory T cell percentages were 4 and 2%, respectively, of normal infection peak values, and no T8 cells were required. It is important to keep in mind that this may be true for infection with Mtb but that different levels of each of the three subsets may be necessary for control of different pathogens (80). These results strongly support the belief that vaccination strategies targeting both $CD4^+$ and $CD8^+$ T cells are likely to be most effective against Mtb infection.

We also determined that it is crucial that the memory T cells be present in the lungs at the time of infection (or shortly thereafter). If memory cells arrived in the lungs by 1 day postchallenge, the vaccination was effective. However, if cells arrived even by 3 days postchallenge, the vaccination was ineffective at clearing bacterial load but served to delay time to latency. There has been extensive

mathematical modeling exploring the generation of CD8$^+$ T cell immune memory (81). In our present work we have assumed that memory cells were already generated by a vaccine and only tested differences between numbers of cells in each subset present. Future work could include the generation as well as maintenance of memory T cell subsets for both CD4$^+$ and CD8$^+$ T cells directly into this model.

The current model incorporates IFN-γ-induced apoptosis of Th1 and CD8$^+$ T cells (both subsets) by activated macrophages and indicates that disease is always accompanied by a delayed Th1 and CTL response due to this activity. We also conclude that vigorous internalization of bacteria (macrophage infection rate) is imperative to infection control. Taken together, these two hypotheses provide a possible explanation of disease outcome, i.e., any mechanism that increases extracellular bacterial turnover beyond a critical point results in an enhanced infected and activated macrophage response. The augmented macrophage response feeds back and results in an excessive killing of Th1 and CTL cells that, in turn, further exacerbates infection. This cycle continues until bacterial load is high enough to overwhelm the system. That event is characterized by a decline in activated macrophage numbers and a simultaneous rise in Th1 and CD8$^+$ T cell numbers to saturable levels. Evidently, extracellular bacterial turnover, macrophage activation, and T cell killing need to be tightly regulated to achieve control over infection.

The model, despite being updated from previous work, is still limited by several assumptions. Some suppositions of the earlier model (15) still hold for the current model, including whether bronchoalveolar lavage is a valid site for deriving experimental numbers for TB (for human data) and whether we model Ag presentation at the site of infection in the lungs instead of the lymph nodes. More importantly, although the model emulates disease progression in primate studies, parameter values include a hybrid of primate and mouse data. Results match well qualitatively with experimental outcomes, and we do observe quantitative differences in some cases. A key strength of the model, however, remains that parameter values can be easily updated when data are available while still providing important qualitative results.

In summary, the results from the updated and inclusive mathematical model provide the opportunity to address challenging and interesting questions regarding the immune response to Mtb. These results can guide vaccine development, provide data on basic immunologic mechanisms in the lung, and open up new avenues of study for experimentalists. In this context, the model can be used to test existing hypotheses as well as identify new factors for study in animal models and humans with tuberculosis.

Appendix

Model equations

In this section, we present the equations comprising the updated ordinary differential equations model of immune system-Mtb dynamics. The model simulates interactions between two bacterial subpopulations, eight cell populations, and five cytokines. Equations 7, 8, 9 and 10 are the new equations for T80, T8, TC, and TNF, respectively. Other equations are similar to those in the study by Wigginton and Kirschner (15), with some minor modifications where we included the affects of these new variables as well as updated biological information regarding IFN-γ-induced apoptosis.

Macrophage dynamics. The equations describing rates of change for the macrophage subpopulations are given by Equations 1–3.

$$\frac{dM_R}{dt} = sr_M + \alpha_{4A}(M_A + w_2M_1) + sr_{4B}\left(\frac{F_\alpha}{F_\alpha + f_8I_{10} + s_{4b}}\right) - k2MR\left(\frac{B_E}{B_E + c_9}\right) - k_3M_R\left(\frac{I_\gamma}{I_\gamma + f_1I_4 + s_1}\right)\left(\frac{B_T + \beta F_\alpha}{B_T + \beta F_\alpha + c_8}\right) - \mu_{MRMR} \quad (1)$$

$$\frac{dM_1}{dt} = k_2M_R\left(\frac{B_E}{B_E + c_9}\right) - k_{17}M_1\left(\frac{B_1^2}{B_1^2 + (NM_1)^2}\right) - k_{14A}M_1\left(\frac{(T_c + w_3T_1)/M_I}{(T_c + w_3T_1)/M_1 + c_4}\right) - k_{14B}M_I\left(\frac{F_\alpha}{F_\alpha + f_9I_{10} + s_{4B}}\right) - k_{52}M_I\left(\frac{(T_c\{T_1/(T_1 + c_{T1})\} + w_1T_1)/M_I}{(T_c\{T_1/(T_1 + c_{T1})\} + w_1T_1)/M_1 + c_{52}}\right) - \mu_{MI}M_I \quad (2)$$

$$\frac{dM_A}{dt} = k_3M_R\left(\frac{I_\gamma}{I_\gamma + f_1I_4 + s_1}\right)\left(\frac{B_T + \beta F_\alpha}{B_T + \beta F_\alpha + c_8}\right) - k_4M_A\left(\frac{I_{10}}{I_{10} + s_8}\right) - \mu_{MA}M_A \quad (3)$$

The rate of change of resting macrophages (Equation 1) includes a source term (sr_M) and a natural death term ($-\mu_{MR}M_R$). This is reasonable, because even in the absence of infection, macrophages undergo constant turnover to maintain an equilibrium value, given by $M_R = sr_M/\mu_{MR}$ (negative control). In the course of infection, additional resting macrophages are recruited in a TNF-dependent fashion (33) at a rate of sr_{4B}, and this process is inhibited by IL-10 (88). We also account for the recruitment of macrophages due to TNF-independent mechanisms such as chemokines secreted primarily by activated and infected macrophages (33) at rates of α_{4A} and $w_2{*}\alpha_{4A}$ ($0 < w_2 < 1$), respectively.

Resting macrophages at the site of infection can become chronically infected at a maximum rate of k_2, which is dependent on the level of infection characterized by the extracellular bacterial load. Macrophages are activated at rate of k_3, which is dependent on two signals: the primary from IFN-γ, and the second either by bacteria or TNF (89). Note that because of the difference in measurement units, TNF is scaled by a factor β. IFN-γ-induced activation is inhibited by IL-4.

Infected macrophages (Equation 2) can be cleared by one of several different mechanisms. Given an average maximal intracellular bacterial carrying capacity of N, we assume that one-half of the infected macrophages burst when the intracellular bacterial load reaches NM_I. This mechanism has a maximal rate of k_{17} and is described by a Hill process. Immune responses also contribute to infected macrophage killing by several mechanisms. Both CD8$^+$ and CD4$^+$ T cells can use the Fas-FasL apoptotic pathway to induce apoptosis in these cells at a maximum rate of k_{14A}. The half-saturation constant c_4 describes the effector-target ratio (T_{total}:M_I) at which this process is half-maximal. TNF can also induce apoptosis by binding to the 55-kDa TNF-receptor (90). This process is down-regulated by IL-10 and occurs at a rate of k_{14B}. Finally, CTL killing by CD8$^+$ and CD4$^+$ T cells happens at a rate of k_{52}. Specifically, CD4$^+$ T cells have a limited contribution, and this is

accounted for by scaling the $CD4^+$ T cell numbers ($0 < w_1 < 1$). $CD8^+$ T cell numbers are scaled by a term accounting for their indirect dependence on $CD4^+$ T cells for effector capability (10).

Activated macrophages are generated from the term in Equation 1 and also undergo natural death at a rate proportional to their number ($-\mu_{MA}M_A$). Activated macrophages can be deactivated (or lose activation status) by IL-10 (91) at a rate of k_4.

T cell dynamics. The equations for T cell dynamics are given by Equations 4–9.

$$\frac{dT_0}{dt} = \alpha_{1A}(M_A + w_2M_1) + sr_{1B}\left(\frac{F_\alpha}{F_\alpha + f_8I_{10} + s_{4b2}}\right) + \alpha_2T_0\left(\frac{M_A}{M_A + c_{15}}\right) - k_6I_{12}T_0\left(\frac{I_\gamma}{I_\gamma(f_1I_4 + f_7I_{10}) + s_1}\right) - k_7T_0\left(\frac{I_4}{I_4 + f_2I_\gamma + s_2}\right) - \mu_{T0}T_0 \quad (4)$$

$$\frac{dT_1}{dt} = \alpha_{3A}(M_A + w_2M_I) + sr_{3B}\left(\frac{F_\alpha}{F_\alpha + f_8I_{10} + s_{4b1}}\right) + k_6I_{12}T_0\left(\frac{I_\gamma}{I_\gamma + (f_1I_4 + f_7I_{10}) + s_1}\right) - \mu_{T\gamma}\left(\frac{I_\gamma}{I_\gamma + c}\right)T_1M_A - \mu_{T1}T_1 \quad (5)$$

$$\frac{dT_2}{dt} = \alpha_{3A2}(M_A + w_2M_I) + sr_{3B2}\left(\frac{F_\alpha}{F_\alpha + f_8I_{10} + s_{4b1}}\right) + k_7T_0\left(\frac{I_4}{I_4 + f_2I_\gamma + s_2}\right) - \mu_{T2}T_2 \quad (6)$$

$$\frac{dT_{80}}{dt} = \alpha_{1A}(M_A + wM_1) + sr_{1B}\left(\frac{F_\alpha}{F_\alpha + f_8I_{10} + s_{4b2}}\right) + \alpha_2T_{80}\left(\frac{M_A}{M_A + c_{15}}\right) - k_6I_{12}T_{80}\left(\frac{I_\gamma}{I_\gamma(f_1I_4 + f_7I_{10}) + s_1}\right) - \mu_{T80}T_{80} \quad (7)$$

$$\frac{dT_8}{dt} = m * \alpha_{3Ac}(M_A + w_2M_I) + m * sr_{3Bc}\left(\frac{F_\alpha}{F_\alpha + f_8I_{10} + s_{4b1}}\right) + m * k_6I_{12}T_{80}\left(\frac{I_\gamma}{I_\gamma(f_1I_4 + f_7I_{10}) + s_1}\right) - \mu_{Tc\gamma}\left(\frac{I_\gamma}{I_\gamma + c_c}\right)T_8M_A - \mu_{T8}T_8 \quad (8)$$

$$\frac{dT_c}{dt} = m * \alpha_{3Ac}(M_A + w_2M_I) + m * sr_{3Bc}\left(\frac{F_\alpha}{F_\alpha + f_8I_{10} + s_{4b1}}\right) + m * k_6I_{12}T_{80}\left(\frac{I_\gamma}{I_\gamma(f_1I_4 + f_7I_{10}) + s_1}\right) - \mu_{Tc\gamma}\left(\frac{I_\gamma}{I_\gamma + c_c}\right)T_cM_A - \mu_{Tc}T_c \quad (9)$$

Similar to resting macrophages, recruitment of T cells is both TNF-independent and TNF-dependent (33). The terms are similar, using different rates for the different T cell subsets (α_{1A}, sr_{1B} for Th0 and T80 cells; α_{3A}, sr_{3B} for Th1 and Th2 cells; and α_{3AC}, sr_{3BC} for $CD8^+$ T cells; respectively). We assume that $CD4^+$ T cells can arrive at the site of infection either as Th0 (majority) or that a small fraction may arrive already differentiated into Th1 or Th2 cells (see Ref. 15 for a complete discussion).

Upon arriving at the site of infection, Th0 cells (Equation 4) can proliferate further in response to signals released by activated macrophages at a rate α_2. Th0 cells can also differentiate into Th1 (Equation 5) and Th2 (Equation 6) cells. Th1 differentiation is controlled by IL-12 and IFN-γ and opposed by IL-4 and IL-10. Th2 differentiation is induced by IL-4 and inhibited by IFN-γ. Th0 cells undergo natural death at a rate of $-\mu_{T0}T_0$). Th1 cells can be killed due to IFN-γ-induced apoptosis in the presence of activated macrophages (37–39) at a rate of $\mu_{T\gamma}$. Both Th1 and Th2 cells die naturally at rates μ_{T1} and μ_{T2}, respectively.

As is the case for $CD4^+$ T cells, we assume that $CD8^+$ T cells can arrive at the site of infection either as T80 (majority) (Equation 7) or that a small fraction may arrive already differentiated into effector cells of either T8 (Equation 8) or TC (Equation 9) type. T80 cells are activated due to interaction with Th1 cells and cytokines and have a natural half-life.

$CD8^+$ T cells also undergo IFN-γ induced apoptosis at a peak rate of $\mu_{Tc\gamma}$ and die at a rate of μ_{Tc}. Because the T8 cells (Equation 8) and Tc cells (Equation 9) are functional subsets of the $CD8^+$ T cell population (see Introduction), the equations are identical for both. We introduce a parameter m that accounts for possible overlap between T8 and TC subsets. Although studies directly assessing cytotoxic capacity and IFN-γ production in the same cells are relatively rare, studies have indicated that perforin expression (or cytotoxic function) and IFN-γ expression can occur in the same cell (30–32). Thus, we allow for a small overlap (10%) here of cell types that perform both functions; hence the value of m is 60%. This assumption is studied further in the paragraph entitled *Role of $CD8^+$ T cells* in *Materials and Methods*.

Cytokine dynamics. Equations 10–14 illustrate cytokine dynamics.

$$\frac{dF_\alpha}{dt} = \alpha_{30}M_I + \alpha_{31}M_A\left(\frac{I_\gamma + \beta_2B_T}{I_\gamma + \beta_2B_T + (f_1I_4 + f_7I_{10}) + s_{10}}\right) + \alpha_{32}T_1 + \alpha_{33}(T_c + T_8) - \mu_{F\alpha}F_\alpha \quad (10)$$

$$\frac{dI_\gamma}{dt} = s_g\left(\frac{B_T}{B_T + c_{10}}\right)\left(\frac{I_{12}}{I_{12} + s_7}\right) + \alpha_{5A}T_1\left(\frac{M_A}{M_A + c_{5B}}\right) + \alpha_{5B}T_8\left(\frac{M_A}{M_A + c_{5A}}\right) + \alpha_{5c}M_I + \alpha_7T_0\left(\frac{I_{12}}{I_{12} + f_4I_{10} + s_4}\right) + \alpha_7T_{80}\left(\frac{I_{12}}{I_{12} + f_4I_{10} + s_4}\right) - \mu_{i\gamma}I_\gamma. \quad (11)$$

$$\frac{dI_{12}}{dt} = s_{12}\left(\frac{B_T}{B_T + c_{230}}\right) + \alpha_{23}M_R\left(\frac{B_T}{B_T + c_{23}}\right) + \alpha_8M_A\left(\frac{s}{s + I_{10}}\right) - \mu_{i12}I_{12} \quad (12)$$

$$\frac{dI_{10}}{dt} = \delta_7M_A\left(\frac{s_6}{I_{10} + f_6I_\gamma + s_6}\right) + \alpha_{16}T_1 + \alpha_{17}T_2 + \alpha_{18}(T_8 + T_c) - \mu_{i10}I_{10} \quad (13)$$

$$\frac{dI_4}{dt} = \alpha_{11}T_0 + \alpha_{12}T_2 - \mu_{i4}I_4 \quad (14)$$

TNF (Equation 10) is produced primarily by infected macrophages (33) at a rate of α_{30}. Activated macrophages secrete TNF at a rate

of α_{31} in response to IFN-γ or bacteria, and this process is inhibited by IL-4. Other sources of TNF are Th1 cells (rate of α_{32}) and CD8$^+$ T cells (rate of α_{33}) (92), and TNF has a given half-life.

IFN-γ (Equation 11) is produced by Th0, Th1, and CD8$^+$ T cells in response to Ag presentation by activated macrophages (30) at rates of α_{5A} and α_{5B}, respectively. Production by Th0 and T80 cells is further enhanced by IL-12 and inhibited by IL-10. Other sources of IFN-γ, such as NK and NKT cells, are also believed to play a role in TB infection (24, 93, 94). Because these sources are not accounted for in the model, we include an extra source term (s_g) dependent on the extent of infection and the IL-12 level. Future work will include these cells to test the roles of NK and NKT cells in the dynamics of TB infection, both as IFN-γ producers and cytotoxic cells.

IL-12 (Equation 12) is produced by resting macrophages at a rate of α_{23} in response to infection (95). Activated macrophages also produce IL-12, and this process is inhibited by IL-10 (95). Dendritic cells are the primary source of IL-12 upon Mtb infection (95) and are accounted for by an infection-dependent source term, s_{12}. Finally, there is a natural half-life for IL-12.

IL-10 (Equation 13) is produced mostly by activated macrophages (95), and this process is opposed by IFN-γ and IL-10 itself at a rate of δ_7. Other sources such as Th1 cells, Th2 cells, and CD8$^+$ T cells produce IL-10 at rates of α_{16}, α_{17}, and α_{18}, respectively.

IL-4 (Equation 14) is produced by Th0 cells at a rate of α_{11}, and Th2 cells at rate of α_{12}. IL-4 has a given half-life of μ_{i4}.

Bacterial dynamics. Equations 15 and 16 illustrate bacterial dynamics.

$$\frac{dB_I}{dt} = \alpha_{19}B_I\left(1 - \frac{B_I^2}{B_I^2 + (NM_I)^2}\right) + k_2\left(\frac{N}{2}\right)M_R\left(\frac{B_E}{B_E + c_9}\right) - k_{17}NM_I\left(\frac{B_I^2}{B_I^2 + (NM_I)^2}\right) - k_{14A}NM_I\left(\frac{(T_C + w_3T_I)/M_I}{(T_C + w_3T_I)/M_I + c_4}\right) - k_{14B}NM_I\left(\frac{F_\alpha}{F_\alpha + f_8I_{10} + S_{4b}}\right) - k_{52}NM_I\left(\frac{(T_C\{T_I/(T_I + c_{TI})\} + w_IT_I)/M_I}{(T_C\{T_I/(T_I + c_{TI})\} + w_IT_I)/M_I + c_{52}}\right) - \mu_IB_I \quad (15)$$

$$\frac{dB_E}{dt} = \alpha_{20}B_E + \mu_IB_I - k_{15}M_AB_E - k_{18}M_RB_E + k_{17}NM_I\left(\frac{B_I^2}{B_I^2 + (NM_I)^2}\right) - k_2\left(\frac{N}{2}\right)M_R\left(\frac{B_E}{B_E + c_9}\right) + k_{14A}N * N_{fracc}M_I\left(\frac{(T_C + w_3T_I)/M_I}{(T_C + w_3T_I)/M_I + c_4}\right) + k_{14B}N * N_{fraca}M_I\left(\frac{F_\alpha}{F_\alpha + f_9I_{10} + s_{4b}}\right) \quad (16)$$

Intracellular bacteria (Equation 15) grow at a maximal rate of α_{19} with logistic Hill kinetics accounting for a maximal carrying capacity of a macrophage. Extracellular bacteria (Equation 16) become intracellular when a macrophage becomes chronically infected at an assumed threshold of $N/2$ bacteria, and, hence, this represents a gain term for the intracellular bacteria. Bursting of macrophages (k_{17}) adds to the extracellular subpopulation. Intracellular bacteria are lost in various proportions due to different killing mechanisms. A corresponding gain in extracellular bacteria depends on the mechanism of killing. Whereas Fas-FasL-induced apoptosis (k_{14A}) releases all intracellular bacteria (N) (26), TNF-induced apoptosis (k_{14B}) eliminates ~50% of the bacteria within the macrophage (90, 96), and this is shown by the N_{fraca} multiplier in the *BE* equation. CTL activity (k_{52}) kills virtually all of the intracellular bacteria (N_{fracc}) due to granulysin action (26) and does not add to the *BE* population. Lastly, we assume that natural death of infected macrophages also releases all intracellular bacteria, and this assumption is modeled as a constant turnover of the bacteria (μ_IB_I) from intracellular to extracellular.

Extracellular bacteria grow at a maximum rate of α_{20}. They are taken up and killed by activated and resting macrophages at rates of k_{15} and k_{18}, respectively.

Parameter estimation

Before simulations can be performed, parameters must be estimated from data or by mathematical means. Values for most model parameters are estimated from published experimental data or data generated by our group. Data from human studies and Mtb experiments are favored over mice and other mycobacterial species, respectively. We also use nonhuman primate data where available. Where no appropriate data are available for a given parameter, we conduct uncertainty analysis to obtain a range within orders of magnitude.

A detailed description of techniques used to evaluate model parameters, as well as a listing of parameters already estimated, can be found in work previously published by our group (15). All parameters newly estimated for the purpose of this work are listed in Table III and have been estimated using approaches similar to those described (15).

Acknowledgments

We are grateful to Dr. Vanja Lazarevic for providing data on CD8$^+$ T cell function in the mouse. We thank Drs. John Chan and Simeone Marino for helpful discussions. We also thank Dr. Brian Murphy and Dongxiao Zhu for early efforts on this project.

Disclosures

The authors have no financial conflict of interest.

References

1. Comstock, G. W. 1982. Epidemiology of tuberculosis. *Am. Rev. Respir. Dis.* 125: 8–15.
2. Flynn, J. L., and J. Chan. 2001. Immunology of tuberculosis. *Annu. Rev. Immunol.* 19: 93–129.
3. Manabe, Y. C., and W. R. Bishai. 2000. Latent *Mycobacterium tuberculosis*: persistence, patience, and winning by waiting. *Nat. Med.* 6: 1327–1329.
4. Flynn, J. L., J. Chan, K. J. Triebold, D. K. Dalton, T. A. Stewart, and B. R. Bloom. 1993. An essential role for interferon γ in resistance to *Mycobacterium tuberculosis* infection. *J. Exp. Med.* 178: 2249–2254.
5. Cooper, A. M., D. K. Dalton, T. A. Stewart, J. P. Griffen, D. G. Russell, and I. M. Orme. 1993. Disseminated tuberculosis in IFN-γ gene-disrupted mice. *J. Exp. Med.* 178: 2243–2248.
6. Flynn, J. L., M. M. Goldstein, J. Chan, K. J. Triebold, K. Pfeffer, C. J. Lowenstein, R. Schreiber, T. W. Mak, and B. R. Bloom. 1995. Tumor necrosis factor-α is required in the protective immune response against *Mycobacterium tuberculosis* in mice. *Immunity* 2: 561–572.
7. Bean, A. G., D. R. Roach, H. Briscoe, M. P. France, H. Korner, J. D. Sedgwick, and W. J. Britton. 1999. Structural deficiencies in granuloma formation in TNF gene-targeted mice underlie the heightened susceptibility to aerosol *Mycobacterium tuberculosis* infection, which is not compensated for by lymphotoxin. *J. Immunol.* 162: 3504–3511.
8. Botha, T., and B. Ryffel. 2003. Reactivation of latent tuberculosis infection in TNF-deficient mice. *J. Immunol.* 171: 3110–3118.
9. Serbina, N. V., and J. L. Flynn. 2001. CD8(+) T cells participate in the memory immune response to *Mycobacterium tuberculosis*. *Infect. Immun.* 69: 4320–4328.

10. Serbina, N. V., V. Lazarevic, and J. L. Flynn. 2001. CD4(+) T cells are required for the development of cytotoxic CD8(+) T cells during *Mycobacterium tuberculosis* infection. *J. Immunol.* 167: 6991–7000.
11. Murray, P. J., and R. A. Young. 1999. Increased antimycobacterial immunity in interleukin-10-deficient mice. *Infect. Immun.* 67: 3087–3095.
12. Mogues, T., M. E. Goodrich, L. Ryan, R. LaCourse, and R. J. North. 2001. The relative importance of T cell subsets in immunity and immunopathology of airborne *Mycobacterium tuberculosis* infection in mice. *J. Exp. Med.* 193: 271–280.
13. Marino, S., and D. E. Kirschner. 2004. The human immune response to *Mycobacterium tuberculosis* in lung and lymph node. *J. Theor. Biol.* 227: 463–486.
14. Marino, S., S. Pawar, C. L. Fuller, T. A. Reinhart, J. L. Flynn, and D. E. Kirschner. 2004. Dendritic cell trafficking and antigen presentation in the human immune response to *Mycobacterium tuberculosis*. *J. Immunol.* 173: 494–506.
15. Wigginton, J. E., and D. Kirschner. 2001. A model to predict cell-mediated immune regulatory mechanisms during human infection with *Mycobacterium tuberculosis*. *J. Immunol.* 166: 1951–1967.
16. Algood, H. M., J. Chan, and J. L. Flynn. 2003. Chemokines and tuberculosis. *Cytokine Growth Factor Rev.* 14: 467–477.
17. Bemelmans, M. H., L. J. van Tits, and W. A. Buurman. 1996. Tumor necrosis factor: function, release, and clearance. *Crit. Rev. Immunol.* 16: 1–11.
18. Brookes, R. H., A. A. Pathan, H. McShane, M. Hensmann, D. A. Price, and A. V. Hill. 2003. $CD8^+$ T cell-mediated suppression of intracellular *Mycobacterium tuberculosis* growth in activated human macrophages. *Eur. J. Immunol.* 33: 3293–3302.
19. Canaday, D. H., R. J. Wilkinson, Q. Li, C. V. Harding, R. F. Silver, and W. H. Boom. 2001. CD4(+) and CD8(+) T cells kill intracellular *Mycobacterium tuberculosis* by a perforin and Fas/Fas ligand-independent mechanism. *J. Immunol.* 167: 2734–2742.
20. Flynn, J. L., M. M. Goldstein, K. J. Triebold, B. Koller, and B. R. Bloom. 1992. Major histocompatibility complex class I-restricted T cells are required for resistance to *Mycobacterium tuberculosis* infection. *Proc. Natl. Acad. Sci. USA* 89: 12013–12017.
21. Harty, J. T., A. R. Tvinnereim, and D. W. White. 2000. $CD8^+$ T cell effector mechanisms in resistance to infection. *Annu. Rev. Immunol.* 18: 275–308.
22. Lazarevic, V., and J. Flynn. 2002. $CD8^+$ T cells in tuberculosis. *Am. J. Respir. Crit. Care Med.* 166: 1116–1121.
23. Pathan, A. A., K. A. Wilkinson, R. J. Wilkinson, M. Latif, H. McShane, G. Pasvol, A. V. Hill, and A. Lalvani. 2000. High frequencies of circulating IFN-γ-secreting CD8 cytotoxic T cells specific for a novel MHC class I-restricted *Mycobacterium tuberculosis* epitope in *M. tuberculosis*-infected subjects without disease. *Eur. J. Immunol.* 30: 2713–2721.
24. Vankayalapati, R., P. Klucar, B. Wizel, S. E. Weis, B. Samten, H. Safi, H. Shams, and P. F. Barnes. 2004. NK cells regulate $CD8^+$ T cell effector function in response to an intracellular pathogen. *J. Immunol.* 172: 130–137.
25. Kamath, A. B., J. Woodworth, X. Xiong, C. Taylor, Y. Weng, and S. M. Behar. 2004. Cytolytic $CD8^+$ T cells recognizing CFP10 are recruited to the lung after *Mycobacterium tuberculosis* infection. *J. Exp. Med.* 200: 1479–1489.
26. Stenger, S., R. Mazzaccaro, K. Uyemura, S. Cho, P. Barnes, J. Rosat, A. Sette, M. Brenner, S. Porcelli, B. Bloom, and R. Modlin. 1997. Differential effects of cytolytic T cell subsets on intracellular infection. *Science* 276: 1684–1687.
27. Stenger, S., D. A. Hanson, R. Teitelbaum, P. Dewan, K. R. Niazi, C. J. Froelich, T. Ganz, S. Thoma-Uszynski, A. Melian, C. Bogdan, et al. 1998. An antimicrobial activity of cytolytic T cells mediated by granulysin. *Science* 282: 121–125.
28. Lalvani, A., R. Brookes, R. J. Wilkinson, A. S. Malin, A. A. Pathan, P. Andersen, H. Dockrell, G. Pasvol, and A. V. Hill. 1998. Human cytolytic and interferon γ-secreting $CD8^+$ T lymphocytes specific for *Mycobacterium tuberculosis*. *Proc. Natl. Acad. Sci. USA* 95: 270–275.
29. Li, L., S. Sad, D. Kagi, and T. R. Mosmann. 1997. CD8Tc1 and Tc2 cells secrete distinct cytokine patterns in vitro and in vivo but induce similar inflammatory reactions. *J. Immunol.* 158: 4152–4161.
30. Lazarevic, V., D. Nolt, and J. L. Flynn. 2005. Long-term control of *Mycobacterium tuberculosis* infection is mediated by dynamic immune responses. *J. Immunol.* 175: 1107–1117.
31. Sad, S., D. Kagi, and T. R. Mosmann. 1996. Perforin and Fas killing by $CD8^+$ T cells limits their cytokine synthesis and proliferation. *J. Exp. Med.* 184: 1543–1547.
32. Valitutti, S., S. Muller, M. Dessing, and A. Lanzavecchia. 1996. Different responses are elicited in cytotoxic T lymphocytes by different levels of T cell receptor occupancy. *J. Exp. Med.* 153: 1917–1921.
33. Algood, H. M., P. L. Lin, D. Yankura, A. Jones, J. Chan, and J. L. Flynn. 2004. TNF influences chemokine expression of macrophages in vitro and that of $CD11b^+$ cells in vivo during *Mycobacterium tuberculosis* infection. *J. Immunol.* 172: 6846–6857.
34. Liu, W., and D. A. Saint. 2002. Validation of a quantitative method for real time PCR kinetics. *Biochem. Biophys. Res. Commun.* 294: 347–353.
35. Mosmann, T. 1983. Rapid colorimetric assay for cellular growth and survival: application to proliferation and cytotoxicity assays. *J. Immunol. Methods* 65: 55–63.
36. Eskandari, M. K., D. T. Nguyen, S. L. Kunkel, and D. G. Remick. 1990. WEHI 164 subclone 13 assay for TNF: sensitivity, specificity, and reliability. *Immunol. Invest.* 19: 69–79.
37. Dalton, D. K., L. Haynes, C. Q. Chu, S. L. Swain, and S. Wittmer. 2000. Interferon γ eliminates responding CD4 T cells during mycobacterial infection by inducing apoptosis of activated CD4 T cells. *J. Exp. Med.* 192: 117–122.
38. Roger, P. M., and L. E. Bermudez. 2001. Infection of mice with *Mycobacterium avium* primes $CD8^+$ lymphocytes for apoptosis upon exposure to macrophages. *Clin. Immunol.* 99: 378–386.
39. Fayyazi, A., B. Eichmeyer, A. Soruri, S. Schweyer, J. Herms, P. Schwarz, and H. J. Radzun. 2000. Apoptosis of macrophages and T cells in tuberculosis-associated caseous necrosis. *J. Pathol.* 191: 417–425.
40. Caruso, A. M., N. Serbina, E. Klein, K. Triebold, B. R. Bloom, and J. L. Flynn. 1999. Mice deficient in CD4 T cells have only transiently diminished levels of IFN-γ, yet succumb to tuberculosis. *J. Immunol.* 162: 5407–5416.
41. Sanchez, M. A., and S. M. Blower. 1997. Uncertainty and sensitivity analysis of the basic reproductive rate: tuberculosis as an example. *Am. J. Epidemiol.* 145: 1127–1137.
42. Helton, J. C., and F. J. Davis. 2002. Illustration of sampling-based methods for uncertainty and sensitivity analysis. *Risk Anal.* 22: 591–622.
43. Zhang, M., Y. Lin, D. V. Iyer, J. Gong, J. S. Abrams, and P. F. Barnes. 1995. T-cell cytokine responses in human infection with *Mycobacterium tuberculosis*. *Infect. Immun.* 63: 3231–3234.
44. van Crevel, R., E. Karyadi, F. Preyers, M. Leenders, B. J. Kullberg, R. H. Nelwan, and J. W. van der Meer. 2000. Increased production of interleukin 4 by $CD4^+$ and $CD8^+$ T cells from patients with tuberculosis is related to the presence of pulmonary cavities. *J. Infect. Dis.* 181: 1194–1197.
45. Tsao, T. C., C. H. Chen, J. H. Hong, M. J. Hsieh, K. C. Tsao, and C. H. Lee. 2002. Shifts of T4/T8 T lymphocytes from BAL fluid and peripheral blood by clinical grade in patients with pulmonary tuberculosis. *Chest* 122: 1285–1291.
46. Tsao, T. C., J. Hong, C. Huang, P. Yang, S. K. Liao, and K. S. Chang. 1999. Increased TNF-α, IL-1 β and IL-6 levels in the bronchoalveolar lavage fluid with the up-regulation of their mRNA in macrophages lavaged from patients with active pulmonary tuberculosis. *Tuber Lung Dis.* 79: 279–285.
47. Pereira, C. B., M. Palaci, O. H. Leite, A. J. Duarte, and G. Benard. 2004. Monocyte cytokine secretion in patients with pulmonary tuberculosis differs from that of healthy infected subjects and correlates with clinical manifestations. *Microbes Infect* 6: 25–33.
48. Morikawa, F., A. Nakano, H. Nakano, F. Oseko, and S. Morikawa. 1989. Enhanced natural killer cell activity in patients with pulmonary tuberculosis. *Jpn. J. Med.* 28: 316–322.
49. Capuano, S. V. III, D. A. Croix, S. Pawar, A. Zinovik, A. Myers, P. L. Lin, S. Bissel, C. Fuhrman, E. Klein, and J. L. Flynn. 2003. Experimental *Mycobacterium tuberculosis* infection of cynomolgus macaques closely resembles the various manifestations of human *M. tuberculosis* infection. *Infect. Immun.* 71: 5831–5844.
50. Silver, R. F., Q. Li, W. H. Boom, and J. J. Ellner. 1998. Lymphocyte-dependent inhibition of growth of virulent *Mycobacterium tuberculosis* H37Rv within human monocytes: requirement for $CD4^+$ T cells in purified protein derivative-positive, but not in purified protein derivative-negative subjects. *J. Immunol.* 160: 2408–2417.
51. Silver, R. F., Q. Li, and J. J. Ellner. 1998. Expression of virulence of *Mycobacterium tuberculosis* within human monocytes: virulence correlates with intracellular growth and induction of tumor necrosis factor α but not with evasion of lymphocyte-dependent monocyte effector functions. *Infect. Immun.* 66: 1190–1199.
52. Rojas, M., L. F. Barrera, G. Puzo, and L. F. Garcia. 1997. Differential induction of apoptosis by virulent *Mycobacterium tuberculosis* in resistant and susceptible murine macrophages: role of nitric oxide and mycobacterial products. *J. Immunol.* 159: 1352–1361.
53. Wong, C. F., W. W. Yew, S. K. Leung, C. Y. Chan, M. Hui, C. Au-Yeang, and A. F. Cheng. 2003. Assay of pleural fluid interleukin-6, tumour necrosis factor-α and interferon-γ in the diagnosis and outcome correlation of tuberculous effusion. *Respir. Med.* 97: 1289–1295.
54. Lin, Y., M. Zhang, F. M. Hofman, J. Gong, and P. F. Barnes. 1996. Absence of a prominent Th2 cytokine response in human tuberculosis. *Infect. Immun.* 64: 1351–1356.
55. Fenhalls, G., A. Wong, J. Bezuidenhout, P. van Helden, P. Bardin, and P. T. Lukey. 2000. In situ production of γ interferon, interleukin-4, and tumor necrosis factor α mRNA in human lung tuberculous granulomas. *Infect. Immun.* 68: 2827–2836.
56. Dannenberg, A. M., Jr. 2003. Macrophage turnover, division and activation within developing, peak and "healed" tuberculous lesions produced in rabbits by BCG. *Tuberculosis (Edinb.)* 83: 251–260.
57. Badovinac, V. P., K. A. Messingham, S. E. Hamilton, and J. T. Harty. 2003. Regulation of $CD8^+$ T cells undergoing primary and secondary responses to infection in the same host. *J. Immunol.* 170: 4933–4942.
58. Hirsch, C. S., Z. Toossi, G. Vanham, J. L. Johnson, P. Peters, A. Okwera, R. Mugerwa, P. Mugyenyi, and J. J. Ellner. 1999. Apoptosis and T cell hyporesponsiveness in pulmonary tuberculosis. *J. Infect. Dis.* 179: 945–953.
59. Law, K., M. Weiden, T. Harkin, K. Tchou-Wong, C. Chi, and W. N. Rom. 1996. Increased release of interleukin-1 β, interleukin-6, and tumor necrosis factor-α by bronchoalveolar cells lavaged from involved sites in pulmonary tuberculosis. *Am. J. Respir. Crit. Care Med.* 153: 799–804.
60. Casarini, M., F. Ameglio, L. Alemanno, P. Zangrilli, P. Mattia, G. Paone, A. Bisetti, and S. Giosue. 1999. Cytokine levels correlate with a radiologic score in active pulmonary tuberculosis. *Am. J. Respir. Crit. Care Med.* 159: 143–148.
61. Scott, H. M., and J. L. Flynn. 2002. *Mycobacterium tuberculosis* in chemokine receptor 2-deficient mice: influence of dose on disease progression. *Infect. Immun.* 70: 5946–5954.
62. Zhang, M., J. Gong, Y. Lin, and P. F. Barnes. 1998. Growth of virulent and avirulent *Mycobacterium tuberculosis* strains in human macrophages. *Infect. Immun.* 66: 794–799.

63. Tsenova, L., E. Ellison, R. Harbacheuski, A. L. Moreira, N. Kurepina, M. B. Reed, B. Mathema, C. E. Barry III, and G. Kaplan. 2005. Virulence of selected *Mycobacterium tuberculosis* clinical isolates in the rabbit model of meningitis is dependent on phenolic glycolipid produced by the bacilli. *J. Infect. Dis.* 192: 98–106.
64. Reed, M. B., P. Domenech, C. Manca, H. Su, A. K. Barczak, B. N. Kreiswirth, G. Kaplan, and C. E. Barry III. 2004. A glycolipid of hypervirulent tuberculosis strains that inhibits the innate immune response. *Nature* 431: 84–87.
65. Gammack, D., S. Ganguli, S. Marino, J. Segovia-Juarez, and D. E. Kirschner. 2005. Understanding the immune response in tuberculosis using different mathematical models and scales. *Multiscale Model. Simul.* 3: 312–345.
66. Dannenberg, A. M., Jr. 1991. Delayed-type hypersensitivity and cell-mediated immunity in the pathogenesis of tuberculosis. *Immunol. Today* 12: 228–233.
67. Shams, H., B. Wizel, S. E. Weis, B. Samten, and P. F. Barnes. 2001. Contribution of CD8(+) T cells to γ interferon production in human tuberculosis. *Infect. Immun.* 69: 3497–3501.
68. Smith, S. M., and H. M. Dockrell. 2000. Role of CD8 T cells in mycobacterial infections. *Immunol. Cell Biol.* 78: 325–333.
69. Cho, S., V. Mehra, S. Thoma-Uszynski, S. Stenger, N. Serbina, R. J. Mazzaccaro, J. L. Flynn, P. F. Barnes, S. Southwood, E. Celis, et al. Antimicrobial activity of MHC class I-restricted CD8$^+$ T cells in human tuberculosis. *Proc. Natl. Acad. Sci. USA* 97: 12210–12215.
70. Mustafa, T., S. Phyu, R. Nilsen, G. Bjune, and R. Jonsson. 1999. Increased expression of Fas ligand on *Mycobacterium tuberculosis*-infected macrophages: a potential novel mechanism of immune evasion by *Mycobacterium tuberculosis*? *Inflammation* 23: 507–521.
71. Kendrick, M. A., and G. W. Comstock. 1981. BCG vaccination and the subsequent development of cancer in humans. *J. Natl. Cancer Inst.* 66: 431–437.
72. Scanga, C. A., V. P. Mohan, K. Yu, H. Joseph, K. Tanaka, J. Chan, and J. L. Flynn. 2000. Depletion of CD4$^+$ T cells causes reactivation of murine persistent tuberculosis despite continued expression of IFN-γ and NOS2. *J. Exp. Med.* 192: 347–358.
73. Tascon, R. E., E. Stavropoulos, K. V. Lukacs, and M. J. Colston. 1998. Protection against *Mycobacterium tuberculosis* infection by CD8 T cells requires production of γ interferon. *Infect. Immun.* 66: 830–834.
74. Cooper, A. M., J. Magram, J. Ferrante, and I. M. Orme. 1997. Interleukin 12 (IL-12) is crucial to the development of protective immunity in mice intravenously infected with *Mycobacterium tuberculosis*. *J. Exp. Med.* 186: 39–45.
75. Mohan, V. P., C. A. Scanga, K. Yu, H. M. Scott, K. E. Tanaka, E. Tsang, M. M. Tsai, J. L. Flynn, and J. Chan. 2001. Effects of tumor necrosis factor α on host immune response in chronic persistent tuberculosis: possible role for limiting pathology. *Infect. Immun.* 69: 1847–1855.
76. Feng, C. G., D. Jankovic, M. Kullberg, A. Cheever, C. A. Scanga, S. Hieny, P. Caspar, G. S. Yap, and A. Sher. 2005. Maintenance of pulmonary Th1 effector function in chronic tuberculosis requires persistent IL-12 production. *J. Immunol.* 174: 4185–4192.
77. van Pinxteren, L. A. H., J. P. Cassidy, B. H. C. Smedegaard, E. M. Agger, and P. Andersen. 2000. Control of latent *Mycobacterium tuberculosis* infection is dependent on CD8 T cells. *Eur. J. Immunol.* 30: 3689–3698.
78. Behar, S. M., C. C. Dascher, M. J. Grusby, C. R. Wang, and M. B. Brenner. 1999. Susceptibility of mice deficient in CD1D or TAP1 to infection with *Mycobacterium tuberculosis*. *J. Exp. Med.* 189: 1973–1980.
79. Laochumroonvorapong, P., J. Wang, C. C. Liu, W. Ye, A. L. Moreira, K. B. Elkon, V. H. Freedman, and G. Kaplan. 1997. Perforin, a cytotoxic molecule which mediates cell necrosis, is not required for the early control of mycobacterial infection in mice. *Infect. Immun.* 65: 127–132.
80. Kaech, S. M., E. J. Wherry, and R. Ahmed. 2002. Effector and memory T-cell differentiation: implications for vaccine development. *Nat. Rev. Immunol.* 2: 251–262.
81. Antia, R., V. V. Ganusov, and R. Ahmed. 2005. The role of models in understanding CD8$^+$ T-cell memory. *Nat. Rev. Immunol.* 5: 101–111.
82. Pace, E., M. Gjomarkaj, M. Melis, M. Profita, M. Spatafora, A. M. Vignola, G. Bonsignore, and C. H. Mody. 1999. Interleukin-8 induces lymphocyte chemotaxis into the pleural space: role of pleural macrophages. *Am. J. Respir. Crit. Care Med.* 159: 1592–1599.
83. Tsukaguchi, K., B. de Lange, and W. H. Boom. 1999. Differential regulation of IFN-γ, TNF-α, and IL-10 production by CD4(+) $\alpha\beta$ TCR$^+$ T cells and Vδ2(+) $\gamma\delta$ T cells in response to monocytes infected with *Mycobacterium tuberculosis*-H37Ra. *Cell Immunol.* 194: 12–20.
84. Rojas, M., M. Olivier, P. Gros, L. F. Barrera, and L. F. Garcia. 1999. TNF-α and IL-10 modulate the induction of apoptosis by virulent *Mycobacterium tuberculosis* in murine macrophages. *J. Immunol.* 162: 6122–6131.
85. Gilbertson, B., J. Zhong, and C. Cheers. 1999. Anergy, IFN-γ production, and apoptosis in terminal infection of mice with *Mycobacterium avium*. *J. Immunol.* 163: 2073–2080.
86. Oddo, M., T. Renno, A. Attinger, T. Bakker, H. R. MacDonald, and P. R. Meylan. 1998. Fas ligand-induced apoptosis of infected human macrophages reduces the viability of intracellular *Mycobacterium tuberculosis*. *J. Immunol.* 160: 5448–5454.
87. Denys, A., I. A. Udalova, C. Smith, L. M. Williams, C. J. Ciesielski, J. Campbell, C. Andrews, D. Kwaitkowski, and B. M. Foxwell. 2002. Evidence for a dual mechanism for IL-10 suppression of TNF-α production that does not involve inhibition of p38 mitogen-activated protein kinase or NF-κB in primary human macrophages. *J. Immunol.* 168: 4837–4845.
88. D'Amico, G., G. Frascaroli, G. Bianchi, P. Transidico, A. Doni, A. Vecchi, S. Sozzani, P. Allavena, and A. Mantovani. 2000. Uncoupling of inflammatory chemokine receptors by IL-10: generation of functional decoys. *Nat. Immunol.* 1: 387–391.
89. Flynn, J. L., and J. Chan. 2001. Tuberculosis: latency and reactivation. *Infect. Immun.* 69: 4195–4201.
90. Keane, J., H. G. Remold, and H. Kornfeld. 2000. Virulent *Mycobacterium tuberculosis* strains evade apoptosis of infected alveolar macrophages. *J. Immunol.* 164: 2016–2020.
91. Bogdan, C., Y. Vodovotz, and C. Nathan. 1991. Macrophage deactivation by interleukin 10. *J. Exp. Med.* 174: 1549.
92. Serbina, N. V., and J. L. Flynn. 1999. Early emergence of CD8(+) T cells primed for production of type 1 cytokines in the lungs of *Mycobacterium tuberculosis*-infected mice. *Infect. Immun.* 67: 3980–3988.
93. Chackerian, A., J. Alt, V. Perera, and S. M. Behar. 2002. Activation of NKT cells protects mice from tuberculosis. *Infect. Immun.* 70: 6302–6309.
94. Junqueira-Kipnis, A. P., A. Kipnis, A. Jamieson, M. G. Juarrero, A. Diefenbach, D. H. Raulet, J. Turner, and I. M. Orme. 2003. NK cells respond to pulmonary infection with *Mycobacterium tuberculosis*, but play a minimal role in protection. *J. Immunol.* 171: 6039–6045.
95. Hickman, S. P., J. Chan, and P. Salgame. 2002. *Mycobacterium tuberculosis* induces differential cytokine production from dendritic cells and macrophages with divergent effects on naive T cell polarization. *J. Immunol.* 168: 4636–4642.
96. Ciaramella, A., A. Cavone, M. B. Santucci, M. Amicosante, A. Martino, G. Auricchio, L. P. Pucillo, V. Colizzi, and M. Fraziano. 2002. Proinflammatory cytokines in the course of *Mycobacterium tuberculosis*-induced apoptosis in monocytes/macrophages. *J. Infect. Dis.* 186: 1277–1282.